



BNXXXX-v0.0
September 13, 2025

Measurement of inclusive $B \rightarrow \Lambda_c$ branching fractions using Belle data and hadronic Full Event Interpretation

Leonardo Benjamin Rizzato¹.

¹*Institute Jožef Stefan, Ljubljana, Slovenia*

Abstract

Inclusive $B \rightarrow \Lambda_c$ branching fractions were measured most recently by BaBar collaboration. However, the measurement still presented a poor accuracy. A more precise measurement of inclusive $B \rightarrow \Lambda_c$ branching fraction could be useful to gain a better confidence on B meson weak decays treatment. With help of the Full Event Interpretation algorihm, it is possible to perform a more precise measurement of inclusive $B \rightarrow \Lambda_c$ branching fractions using Belle data set.

Contents

1	Introduction	1
1.1	Analysis Setup	1
1.2	Datasets	1
2	Event selection and reconstruction	3
2.1	B_{tag} reconstruction	3
2.2	Λ_c reconstruction	3
2.3	Wrongly reconstructed B_{tag} candidates	4
2.4	Signal selection optimization	6
2.4.1	$B^- \rightarrow \Lambda_c^+$ decays	7
2.4.2	$B^+ \rightarrow \Lambda_c^+$ decays	10
2.4.3	$\bar{B}^0 \rightarrow \Lambda_c^+$ decays	14
2.4.4	$B^0 \rightarrow \Lambda_c^+$ decays	18
3	2D simultaneous fit	21
3.1	Probability Density Functions (PDFs) for the two dimensional fit	21
3.1.1	Total Signal fits	21
3.1.2	Mbc peaking and flat background	23
3.1.3	Crossfeed background	25
3.1.4	Continuum background	27
3.2	Two dimensional fit on Monte Carlo	35
3.2.1	Fit results for $B^- \rightarrow \Lambda_c^+$ decays	37
3.2.2	Fit results for $B^- \rightarrow \bar{\Lambda}_c^-$ decays	39
3.2.3	Fit results for $\bar{B}^0 \rightarrow \Lambda_c^+$ decays	41
3.2.4	Fit results for $\bar{B}^0 \rightarrow \bar{\Lambda}_c^-$ decays	43
3.2.5	Fit residuals	44
3.2.6	toy Monte Carlo study	46
4	B_{tag} fit	48
4.1	Probability Density Functions (PDFs) for the B_{tag}	48
4.1.1	Total Signal fits	48
4.1.2	Crossfeed PDF	50
4.1.3	Continuum PDF	53

4.2	B_{tag} fit	54
4.2.1	Fit results for $B^- \rightarrow \Lambda_c^+$ decays	54
4.2.2	Fit results for $B^- \rightarrow \bar{\Lambda}_c^-$ decays	55
4.2.3	Fit results for $\bar{B}^0 \rightarrow \Lambda_c^+$ decays	56
4.2.4	Fit results for $\bar{B}^0 \rightarrow \bar{\Lambda}_c^+$ decays	57
5	Efficiencies	59
5.0.1	Λ_c efficiency	59
5.0.2	$B^- \rightarrow \Lambda_c^+$ decays	59
5.0.3	$B^- \rightarrow \bar{\Lambda}_c^-$ decays	60
5.0.4	$\bar{B}^0 \rightarrow \Lambda_c^+$ decays	60
5.0.5	$\bar{B}^0 \rightarrow \bar{\Lambda}_c^-$ decays	60
6	Branching ratio	61
	References	62

¹ Chapter 1

² Introduction

³ Inclusive B meson baryonic decays with a Λ_c baryon in the final state are the most
⁴ abundant, due to a relatively large V_{cb} element of the CKM matrix. The *BaBar* experiment
⁵ measured their branching fractions to be around the percent level (see ref. [1]). However, the
⁶ branching fractions were determined with big uncertainties: nearly 50% on the measured
⁷ values or, in the case of the $B^0 \rightarrow \Lambda_c^+$ decay, only an upper limit could be established.
⁸ A more precise measurement of inclusive $B \rightarrow \Lambda_c$ branching fractions may shed light on
⁹ the appropriateness of B meson weak decays treatment, particularly of strong interaction
¹⁰ effects modelling. Predictions for inclusive branching fractions are given, for example, in
¹¹ ref. [2] or in [3] for $B \rightarrow \Lambda_c p$ decays.

¹² Exploiting the Full Event Interpretation (FEI) algorithm, developed for the Belle
¹³ II experiment, it may be possible to perform a more precise measurement of inclusive
¹⁴ $B \rightarrow \Lambda_c$ branching fractions, using the full Belle data set. A more precise measurement
¹⁵ may also trigger further research on currently scarce theory predictions for B meson decays
¹⁶ to charm baryons.

¹⁷ 1.1 Analysis Setup

¹⁸ The reconstruction is performed with **BASF2** release 05-02-03 together with the **b2bii**
¹⁹ package in order to convert the *Belle* MDST files (**BASF** data format) to *Belle II* MDST files
²⁰ (**BASF2** data format). The FEI version used is **FEI_B2BII_light-2012-minos**.

²¹ 1.2 Datasets

²² The Belle detector acquired a dataset of about $L_0 \approx 710 fb^{-1}$ of integrated luminosity in
²³ its lifetime at the $\Upsilon(4S)$ energy of 10.58 GeV, which corresponds to about $771 \times 10^6 B\bar{B}$
²⁴ meson pairs. Additionally, several streams of Monte-Carlo (MC) samples were produced,
²⁵ where each stream of MC corresponds to the same amount of data that was taken with
²⁶ the detector. No specific signal MC was used: instead of producing dedicated signal MC

²⁷ samples, the samples were obtained by filtering the decays of interest from the generic
²⁸ on-resonance MC samples. The following samples were used in this analysis:

- ²⁹ • data
- ³⁰ • MC - 6 streams of B^+B^- and $B^0\bar{B}^0$ (denoted as **charged** and **mixed**) for signal
³¹ decays and backgrounds (if more of the in total existing 10 streams is used it is
³² explicitly specified throughout this note).
 - ³³ - 6 streams of $q\bar{q}$ produced at $\Upsilon(4S)$ resonance energy
 - ³⁴ - 6 streams of $q\bar{q}$ produced at 60 MeV below $\Upsilon(4S)$ resonance energy, where each
³⁵ stream corresponds to $1/10 \times L_0$.

³⁶

³⁷ **Chapter 2**

³⁸ **Event selection and reconstruction**

³⁹ In this chapter the procedure for reconstruction of the events where one B meson decays
⁴⁰ inclusively to a Λ_c baryon and the accompanying B meson decays hadronically is illustrated.

⁴¹ **2.1 B_{tag} reconstruction**

⁴² The FEI is an exclusive tagging algorithm that uses machine learning to reconstruct
⁴³ B meson decay chains and calculates the probability that these decay chains correctly
⁴⁴ describe the true process. In this analysis only hadronically reconstructed decay chains
⁴⁵ are considered. The training called `FEI_B2BII_light-2012-minos` is used. Tag-side B
⁴⁶ meson candidates are required to have a beam-constrained mass greater than $5.22 \text{ GeV}/c^2$
⁴⁷ and $-0.15 < \Delta E < 0.07 \text{ GeV}$.

⁴⁸ In the case of multiple candidates in the same event, the candidate with the highest
⁴⁹ SignalProbability (the signal probability calculated by FEI using FastBDT) is chosen. To
⁵⁰ suppress the background consisting of B^0 events misreconstructed as B^+ (and vice-versa)
⁵¹ from neutral (charged) decays also a B^0 (B^+) candidate is reconstructed with FEI and if
⁵² its SignalProbability is higher than the charged (neutral) reconstructed B meson, the event
⁵³ is discarded. This constitutes a sort of crossfeed-veto, rejecting part of events belonging
⁵⁴ to the other typology of decays of interest: for example in the case one is interested
⁵⁵ in reconstructing $B^{+/-}$ decays and the event actually contains B^0/\bar{B}^0 decays, the FEI
⁵⁶ reconstructed neutral B meson candidate most likely presents a higher SignalProbability
⁵⁷ than the charged FEI reconstructed candidate.

⁵⁸ **2.2 Λ_c reconstruction**

⁵⁹ In the *rest of event* (ROE) of the reconstructed B_{tag} meson, to select $\Lambda_c \rightarrow pK\pi$ signal
⁶⁰ candidates, the following event selection criteria are applied (same PID cuts were used for
⁶¹ example in the Belle Note 1521 https://belle.kek.jp/secured/belle_note/gn1521/BN_v1.pdf). Charged tracks with the impact parameters perpendicular to and along the
⁶² nominal interaction point (IP) are required to be less than 2 cm and 4 cm respectively
⁶³

64 ($dr < 2$ cm and $|dz| < 4$ cm).
 65 The pion tracks are required to be identified with $\frac{\mathcal{L}_\pi}{\mathcal{L}_K + \mathcal{L}_\pi} > 0.6$. The kaon tracks are
 66 required to be identified with $\frac{\mathcal{L}_K}{\mathcal{L}_K + \mathcal{L}_\pi} > 0.6$, and the proton/anti-proton tracks are
 67 required to be identified with $\frac{\mathcal{L}_{p/\bar{p}}}{\mathcal{L}_K + \mathcal{L}_{p/\bar{p}}} > 0.6$ and $\frac{\mathcal{L}_{p/\bar{p}}}{\mathcal{L}_\pi + \mathcal{L}_{p/\bar{p}}} > 0.6$, where the $\mathcal{L}_{\pi,K,p/\bar{p}}$ are the
 68 likelihoods for pion, kaon, proton/anti-proton, respectively, determined using the ratio of
 69 the energy deposit in the ECL to the momentum measured in the SVD and CDC, the
 70 shower shape in the ECL, the matching between the position of charged track trajectory
 71 and the cluster position in the ECL, the hit information from the ACC and the dE/dx
 72 information in the CDC.
 73 For the Λ_c candidates a vertex fit is performed with **TreeFitter**, requiring it to converge.
 74 If there are more than one Λ_c combination, then the best candidate based on the χ^2
 75 probability is chosen. The Λ_c signal region is defined to be $|M_{\Lambda_c} - m_{\Lambda_c}| < 20$ MeV/ c^2 (\sim
 76 3σ), here m_{Λ_c} is the nominal mass of m_{Λ_c} .

77

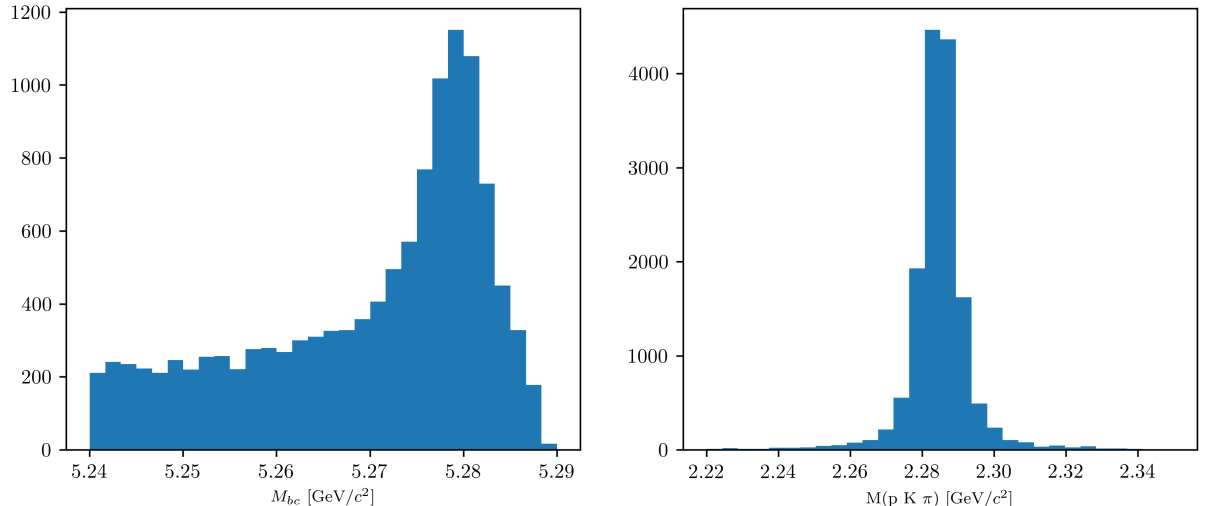


Figure (2.1) M_{bc} and $M(pK\pi)$ distributions of B_{tag} and Λ_c candidates reconstructed in the signal sample.

78 2.3 Wrongly reconstructed B_{tag} candidates

79 In the case of the signal sample the distributions for the beam-constrained mass M_{bc} and
 80 for the correctly reconstructed Λ_c candidates, look like in Fig. 2.1. If one then investigates
 81 the M_{bc} distribution of the B_{tag} candidates reconstructed with FEI, it can be seen that
 82 there is a peaking structure for wrongly reconstructed B mesons (as in Fig. 2.2), according
 83 to the BASF2 internal truth matching variable **isSignal**. It is obvious from this that the
 84 BASF2 internal truth matching variable cannot be used to separate properly the signal
 85 events in correctly and wrongly reconstructed B mesons. In the study BELLE2-NOTE-TE-

86 2021-026 <https://docs.belle2.org/record/2711/files/BELLE2-NOTE-TE-2021-026.pdf>
87 a possible solution was found developing new variables that can be used for an
88 improved truth matching for the FEI (those variables were added to a newer BASF2
89 release than the one used for this study). In the present study instead a more "traditional"
90 approach was adopted: fitting the M_{bc} distribution with a sum of PDFs that account for the
91 flat (background) component and the peaking (signal) component. The first component
92 represents the combinatorial background, i.e. B mesons that were mis-reconstructed,
93 and therefore those events are denoted from now on as "**misreconstructed signal**".
94 The peaking component represents the correctly reconstructed signal events in M_{bc} and
95 therefore denoted from now on as "**reconstructed signal**". Only the second one is then
96 considered for the signal yield, while the first is counted as a background. To validate this
97 method a control decay study was performed on the flavor correlated $B^+ \rightarrow \bar{D}^0$ channel.

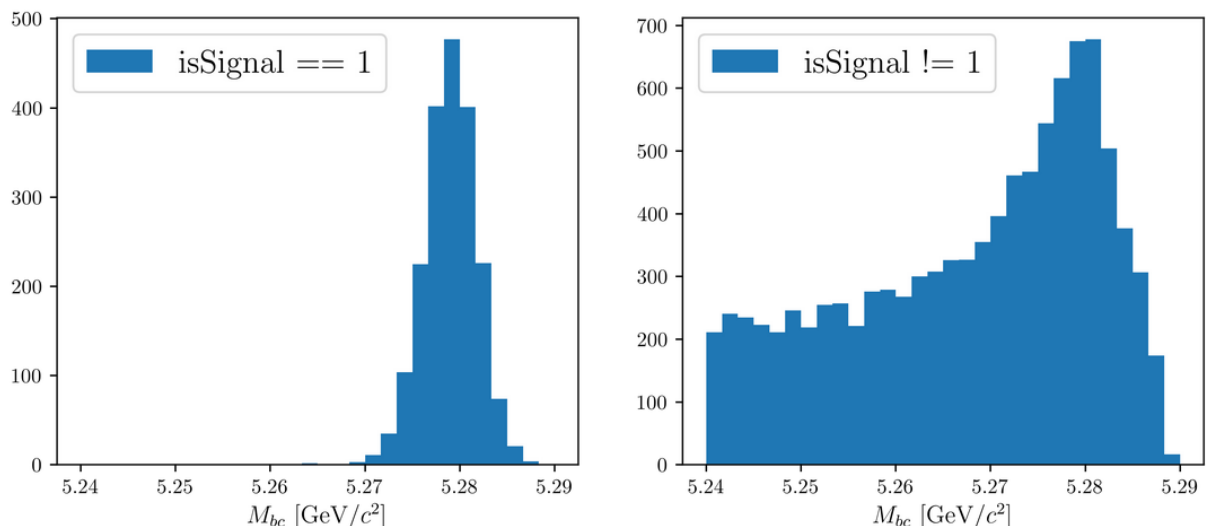


Figure (2.2) M_{bc} distribution of B_{tag} candidates reconstructed in the signal sample, truth-matched (on the left) and not (on the right).

98 2.4 Signal selection optimization

99 To further enhance the purity of the signal decays, an optimization procedure is adopted
100 to determine optimal cuts for a set of variables for each decay mode under investigation
101 by this study. The cuts on the following variables are optimized:

- 102 • *foxWolframR2*: the event based ratio of the 2-nd to the 0-th order Fox-Wolfram
103 moments
- 104 • SignalProbability: the already mentioned signal probability calculated by FEI using
105 FastBDT
- 106 • $p_{CMS}^{\Lambda_c}$: momentum of the Λ_c candidates in the center of mass system

107 The optimization is based on the Figure Of Merit (FOM): $FOM = \frac{S}{\sqrt{S+B}}$
108 Where S and B are respectively signal and background events in the signal region:

109 $M_{bc} > 5.27 \text{ GeV}/c^2$, $2.2665 < M(pK\pi) < 2.3065 \text{ GeV}/c^2$.

110 Due to the issue reported in Sec. 2.3, to separate signal events that peak in M_{bc} from
111 the ones that are not (which are then categorized as background events), the events
112 reconstructed in the signal sample are fitted with a sum of Crystal Ball function and
113 Argus for each cut value on the corresponding variable to optimize (as in Fig. 2.3).

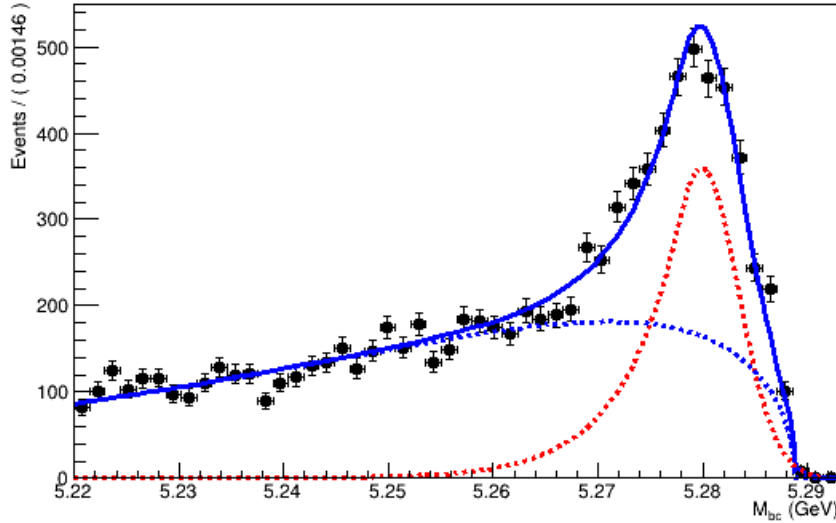


Figure (2.3) Example of a fit used to separate the correctly reconstructed B mesons (described by the red dotted Crystal Ball function) from the wrongly reconstructed ones (described by the blue dotted Argus function).

114 The next sections illustrate the procedure for each of the four decay channels.

115 **2.4.1 $B^- \rightarrow \Lambda_c^+$ decays**

116 Here below the procedure of optimized signal selection of charged correlated decays is
117 presented.

118 First, in order to suppress the continuum background the cut on *foxWolframR2* is
119 optimized. Fig. 2.4 shows the *foxWolframR2* distributions for signal and continuum
120 events.

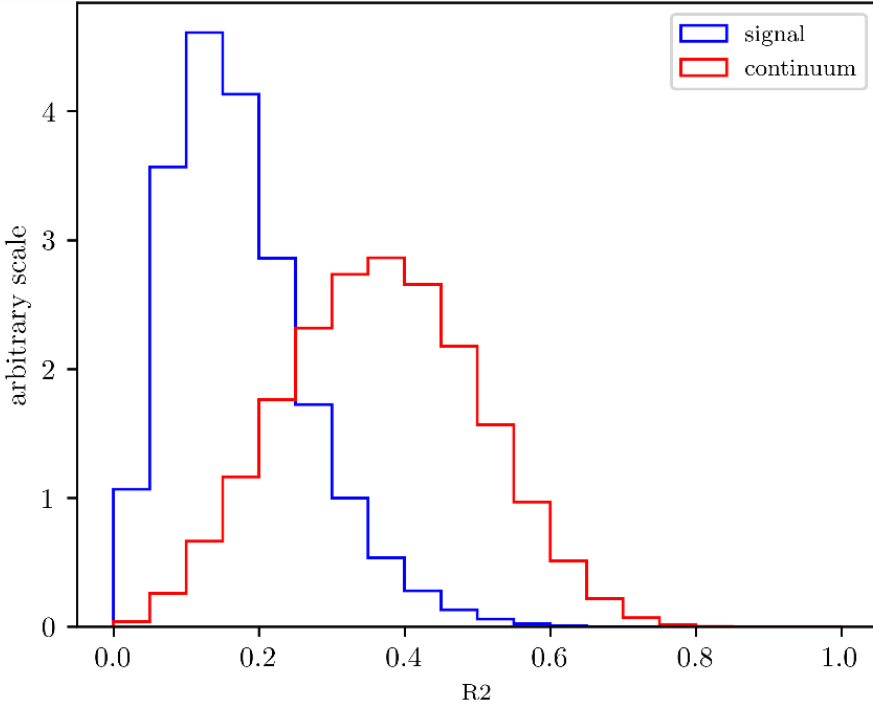


Figure (2.4) Distribution of the *foxWolframR2* variable for signal and continuum background events.

121 With the optimized cut *foxWolframR2* < 0.27 (corresponding to the maximum of
122 the FOM curve shown in Fig. 2.5), the cut on SignalProbability is optimized in the same
123 way (see Fig. 2.6).

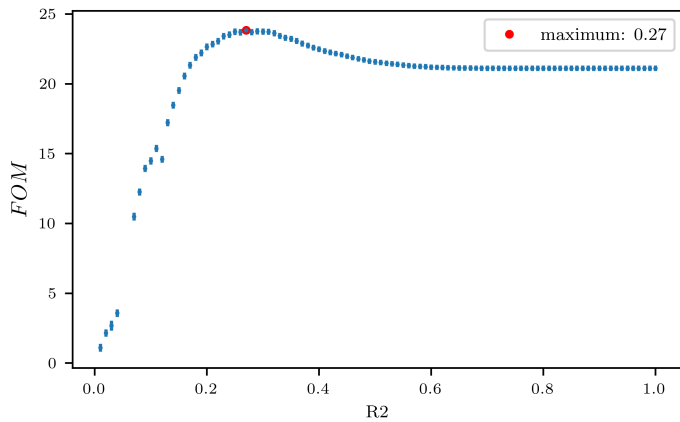


Figure (2.5) Figure of Merit values calculated at several cuts on the *foxWolframR2* variable

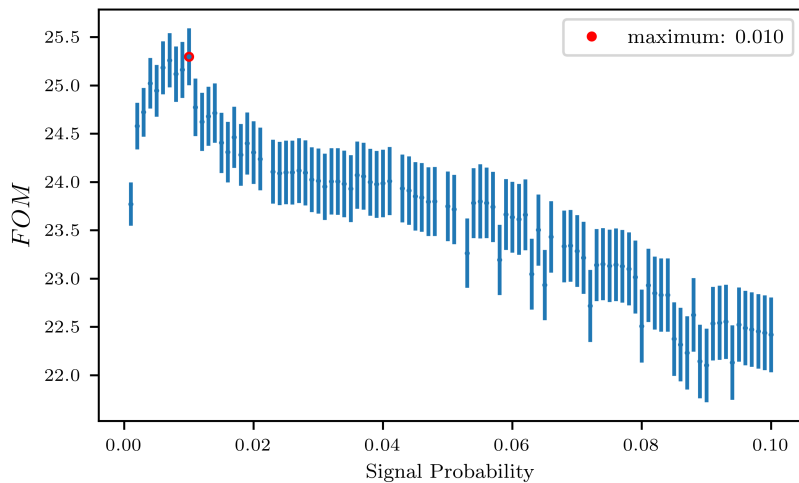


Figure (2.6) Figure of Merit values calculated at several cuts on the *SignalProbability* variable

124 With the optimized cut *SignalProbability* > 0.01, the cut on *foxWolframR2* variable is
 125 rechecked (Fig. 2.7). Being the maximum values fluctuating around *foxWolframR2* < 0.3,
 126 this cut is the one finally chosen for this variable.

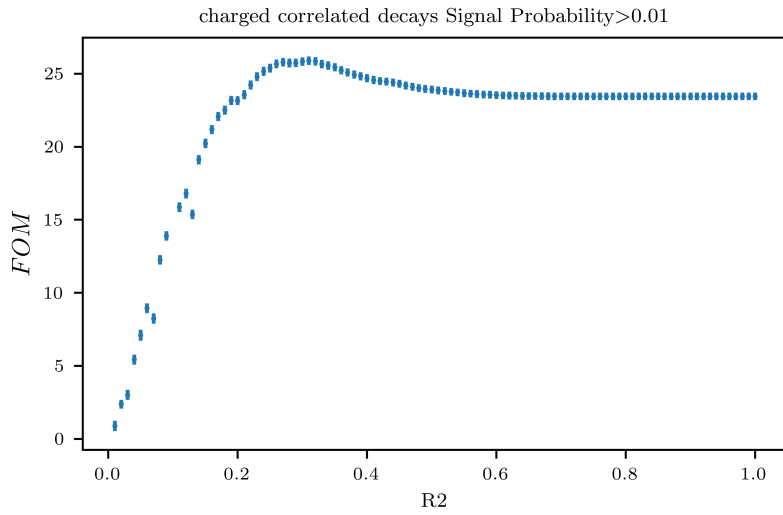


Figure (2.7) Figure of Merit values calculated at several cuts on the *foxWolframR2* variable

127 With the optimized cuts on SignalProbability and *foxWolframR2* variable, the cut
 128 on $p_{CMS}^{\Lambda_c}$ is optimized

129

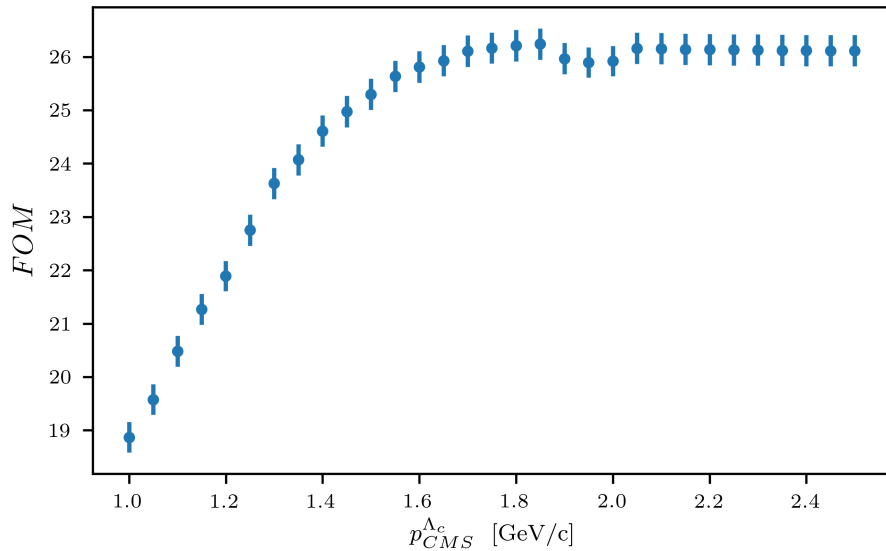


Figure (2.8) Figure of Merit values calculated at several cuts on the momentum of the Λ_c candidates in the center of mass system

130 From Fig. 2.8 one can see that with values of the cut above $p_{CMS}^{\Lambda_c} < 1.8$ GeV/c^2 a
 131 plateau of maximum FOM values is reached. But such a cut would still be useful to reject

¹³² some background events as one can see from Fig. 2.9.

¹³³ Finally the optimized selection cuts are:

¹³⁴ • $\text{foxWolframR2} < 0.3$

¹³⁵ • $\text{SignalProbability} > 0.01$

¹³⁶ • $p_{CMS}^{\Lambda_c} < 1.8 \text{ GeV}/c$

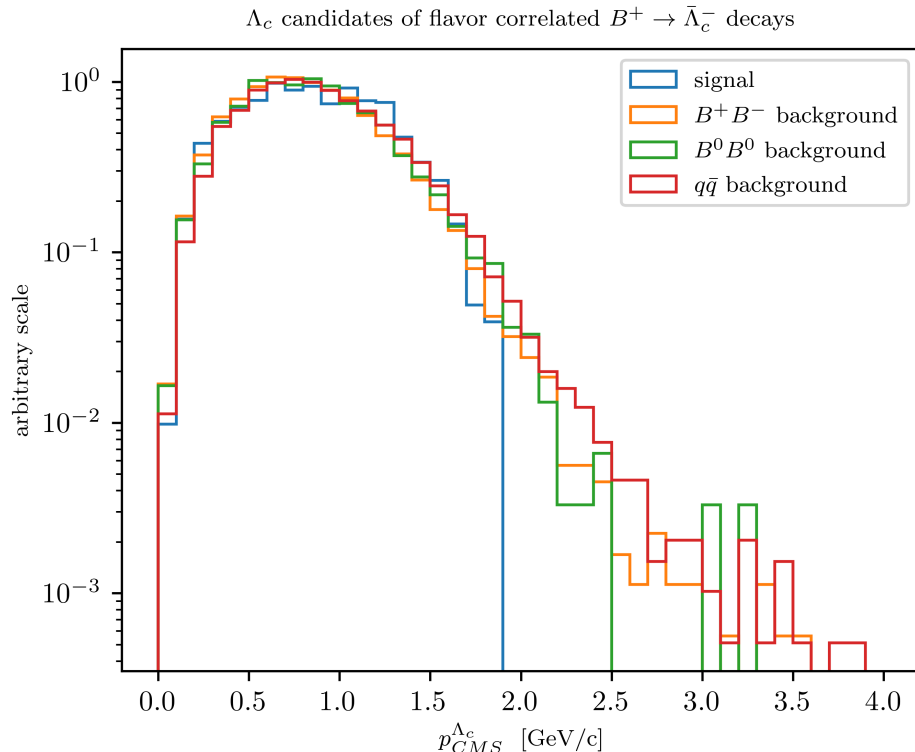


Figure (2.9) Distribution of Λ_c candidates momenta in the center of mass system

¹³⁷ 2.4.2 $B^+ \rightarrow \Lambda_c^+$ decays

¹³⁸ For anticorrelated decays, the same foxWolframR2 cut is defined after the optimization
¹³⁹ procedure (see Fig. 2.13).

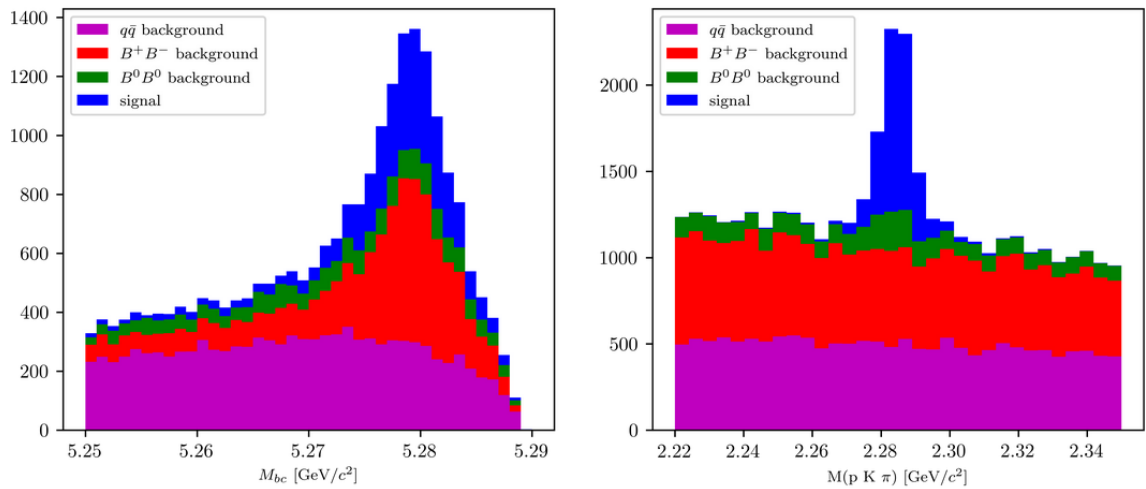


Figure (2.10) Distribution of M_{bc} (left) and invariant mass of charged correlated Λ_c candidates (right), in the signal region after the above mentioned selection cuts.

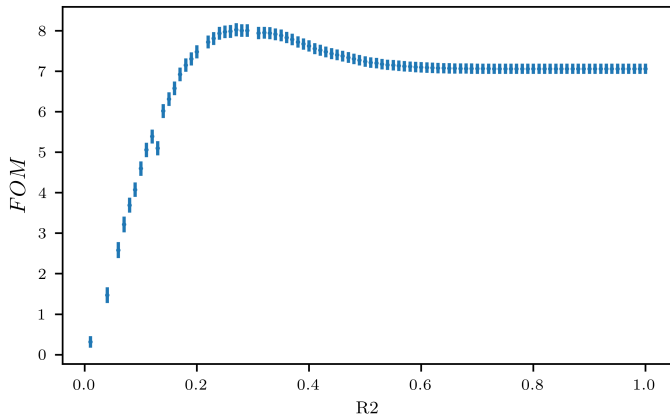


Figure (2.11) Figure of Merit values calculated at several cuts on the $foxWolframR2$ variable

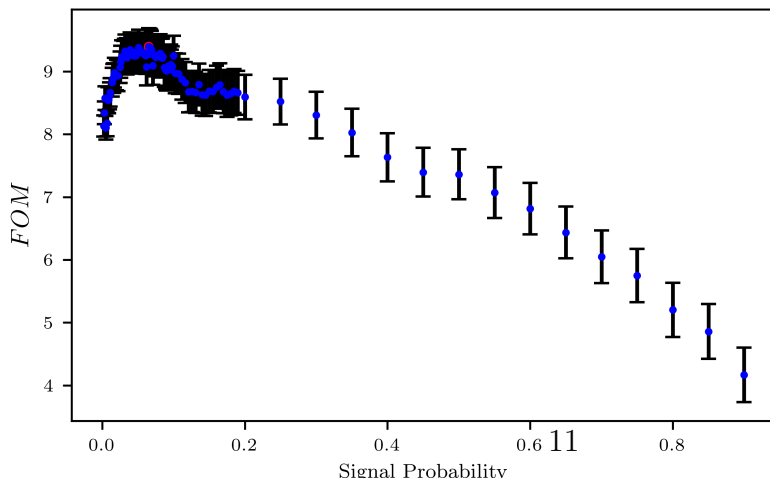


Figure (2.12) Figure of Merit values calculated at several cuts on the SignalProbability variable

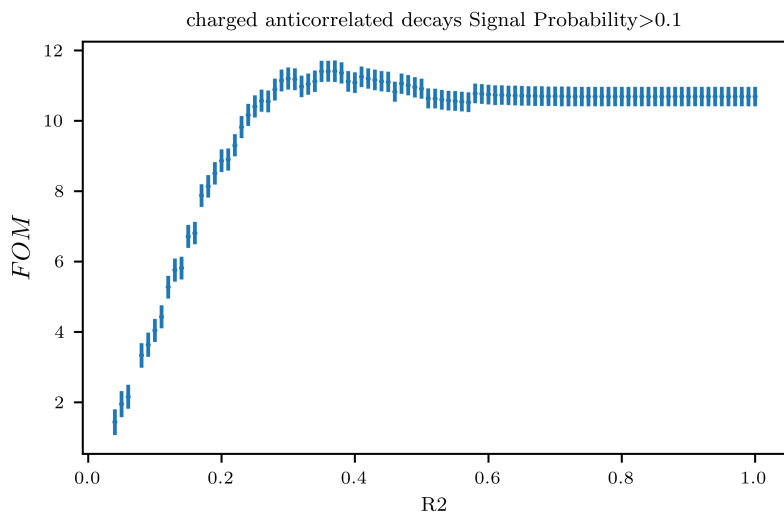


Figure (2.13) Figure of Merit values calculated at several cuts on the *foxWolframR2* variable

¹⁴⁰ With the optimized cuts on SignalProbability and *foxWolframR2* variable, the cut
¹⁴¹ on $p_{CMS}^{\Lambda_c}$ is selected.

¹⁴²

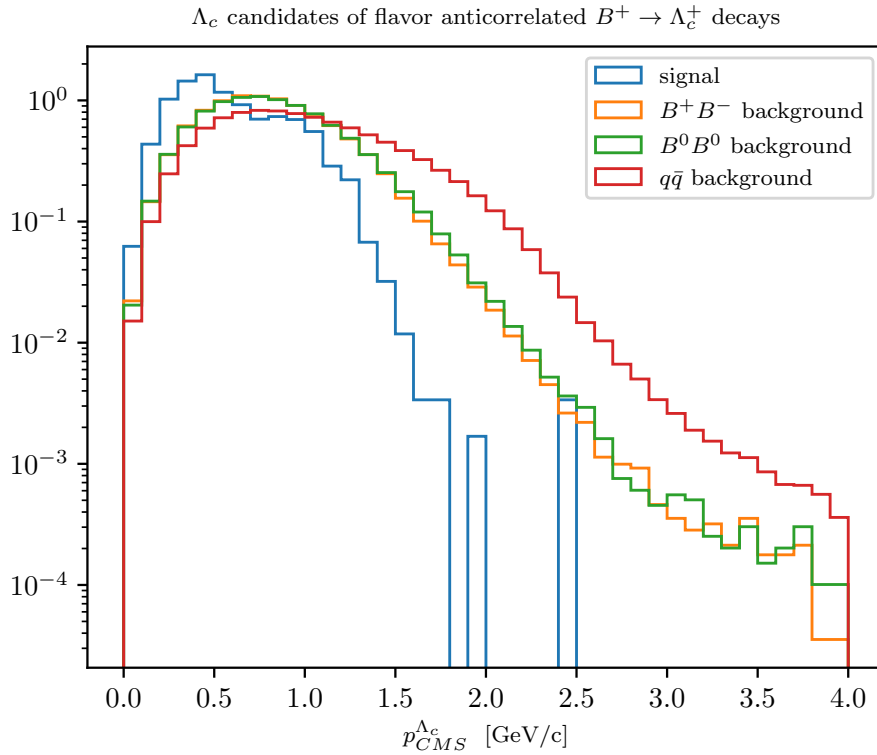


Figure (2.14) Distribution of Λ_c candidates momenta in the center of mass system

¹⁴³ The final optimized selection cuts are:

¹⁴⁴ • $foxWolframR2 < 0.3$

¹⁴⁵ • SignalProbability > 0.1

¹⁴⁶ • $p_{CMS}^{\Lambda_c} < 1.5$ GeV/c

¹⁴⁷ Fig. 2.15 shows the projections of the M_{bc} and $M(pK\pi)$ distributions.

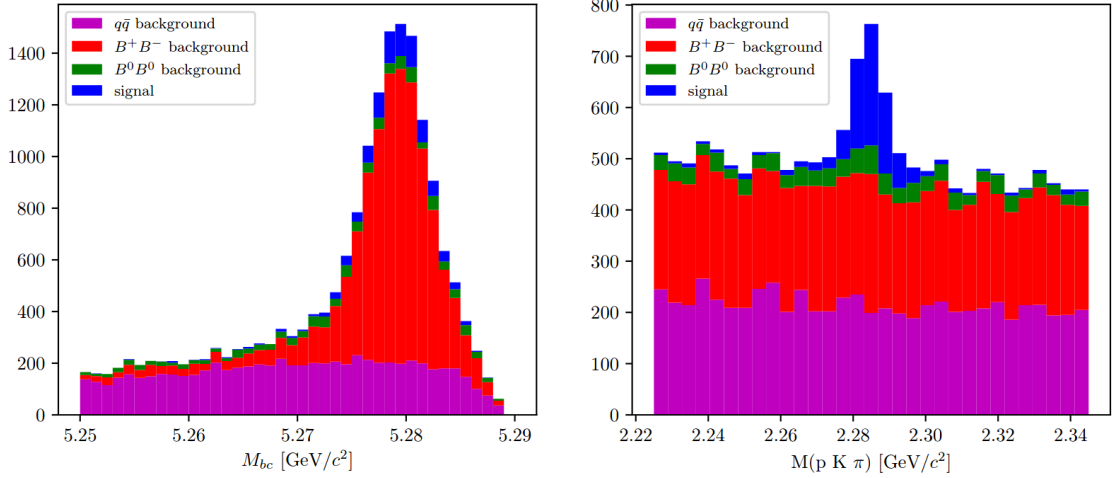


Figure (2.15) Distribution of M_{bc} (left) and invariant mass of charged correlated Λ_c candidates (right), in the signal region after the above mentioned selection cuts.

¹⁴⁸ 2.4.3 $\bar{B}^0 \rightarrow \Lambda_c^+$ decays

¹⁴⁹ Also for neutral correlated decays, first the cut on *foxWolframR2* is optimized.

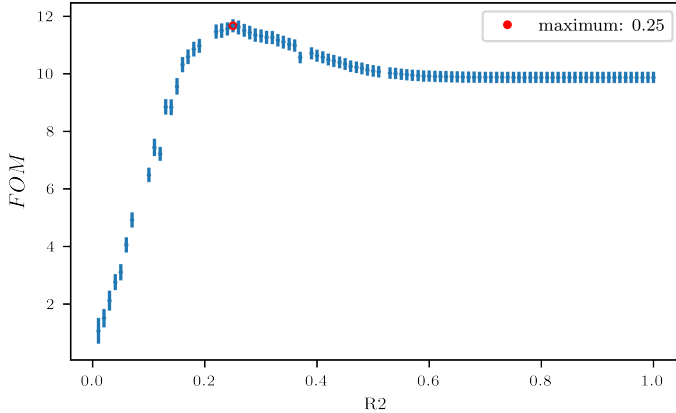


Figure (2.16) Figure of Merit values calculated at several cuts on the *foxWolframR2* variable

¹⁵⁰ The cut suggested by Fig. 2.16, $foxWolframR2 < 0.27$, is used to define the cut on ¹⁵¹ the SignalProbability variable. From Fig. 2.17, it seems the optimal cut maximizing the ¹⁵² *FOM* would be around 0.05. If one zooms like in Fig. 2.18 one can see that there is a ¹⁵³ sort of plateau starting around 0.03 and ending after values around 0.11, where the values ¹⁵⁴ fluctuate within statistical uncertainties around *FOM* = 13. In this case, a legitimate ¹⁵⁵ choice is to use the most stringent cut (*SignalProbability* > 0.11) being the *FOM* same ¹⁵⁶ but rejecting more background events.

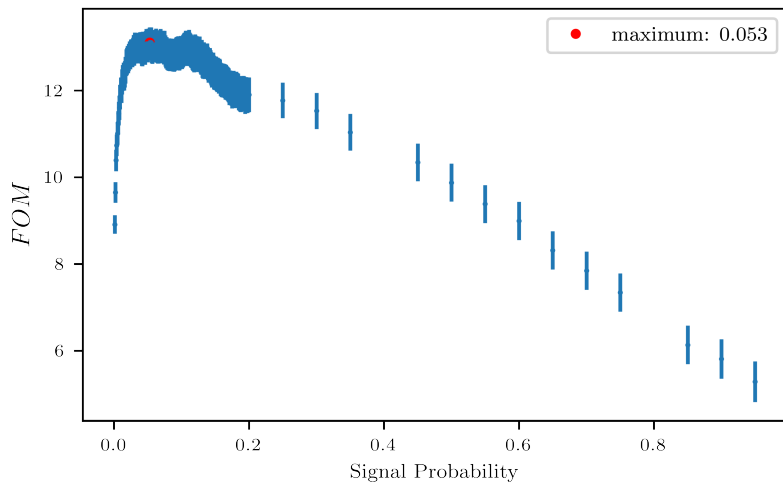


Figure (2.17) Figure of Merit values calculated at several cuts on the SignalProbability variable

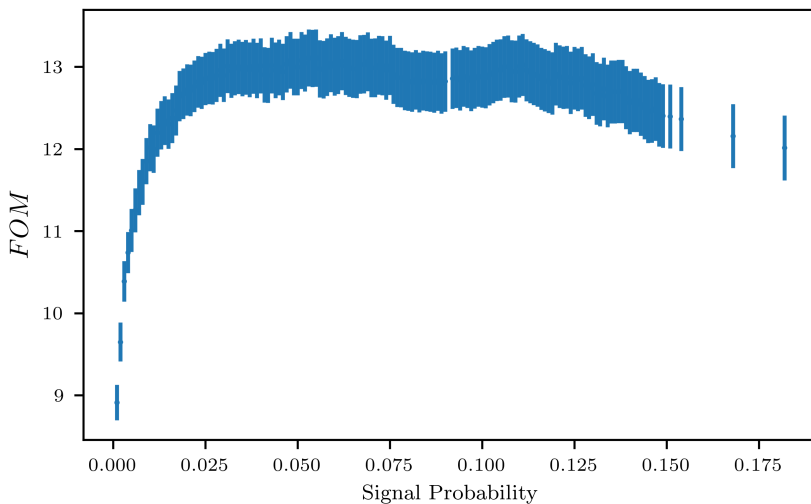


Figure (2.18) Figure of Merit values calculated at several cuts on the SignalProbability variable

157 The *FOM* curve for the *foxWolframR2* variable is rechecked applying the chosen
 158 cut on *SignalProbability* (Fig. 2.19). As done in the other cases the final cut chosen is
 159 $\text{foxWolframR2} < 0.3$

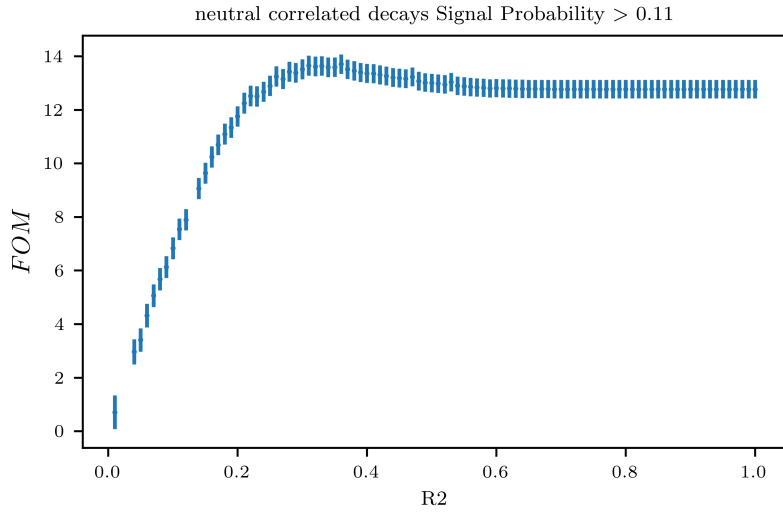


Figure (2.19) Figure of Merit values calculated at several cuts on the *foxWolframR2* variable

160 Using now the two optimized cuts to check the *FOM* curve for the momenta a plateau
 161 appears for cuts starting from values around $p_{CMS}^{\Lambda_c} < 1.7$ GeV/c (see Fig. 2.20). In fact,
 162 around that value the level of background becomes significantly higher compared to the
 163 amount o signal events as one can see in Fig. 2.21

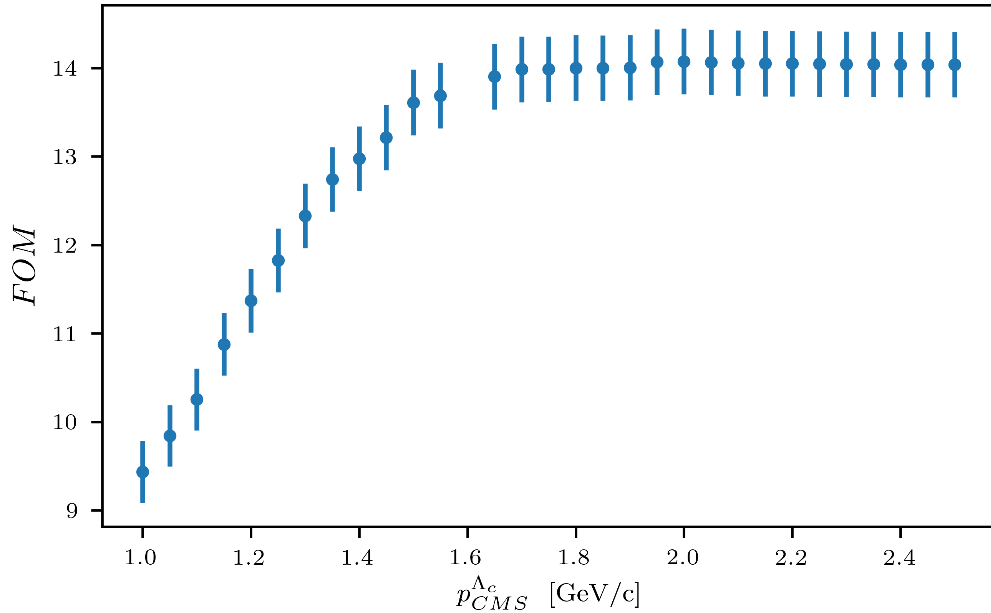


Figure (2.20) Figure of Merit values calculated at several cuts on the momentum of the Λ_c candidates in the center of mass system

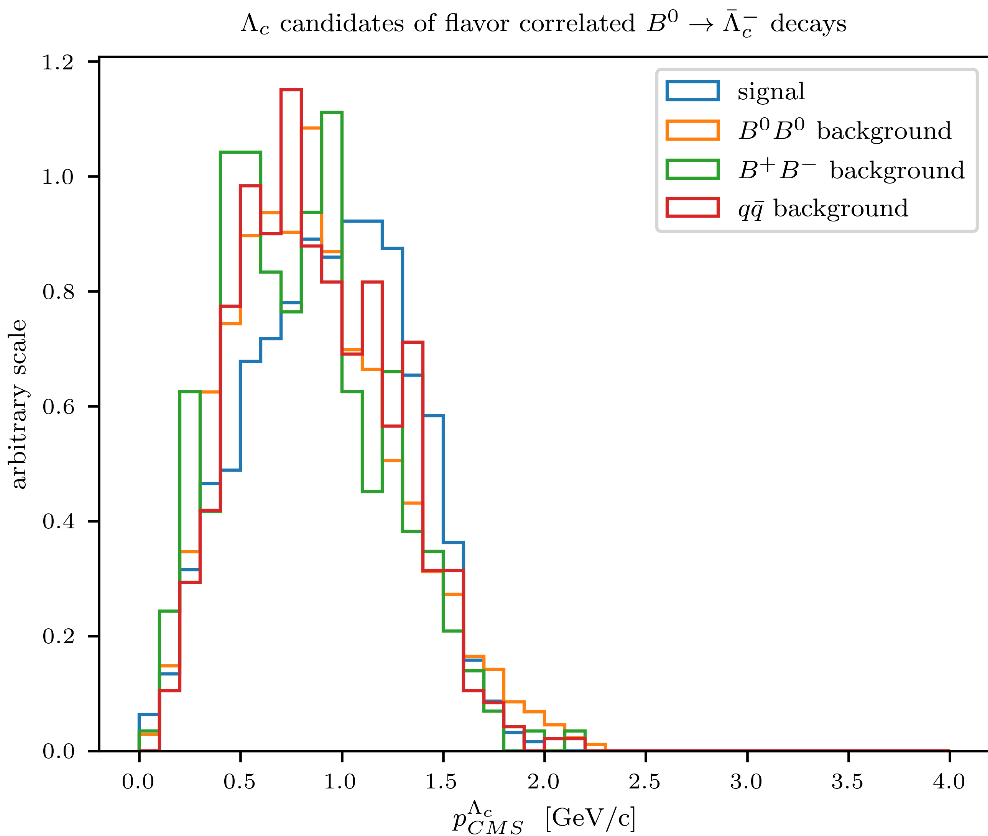


Figure (2.21) Distribution of Λ_c candidates momenta in the center of mass system

164 Fig. 2.22 shows the M_{bc} and $M(pK\pi)$ distributions after applying the following set of
 165 cuts:

- 166 • $foWolframR2 > 0.3$
- 167 • SignalProbability > 0.11
- 168 • $p_{CMS}^{\Lambda_c} < 1.7$ GeV/c

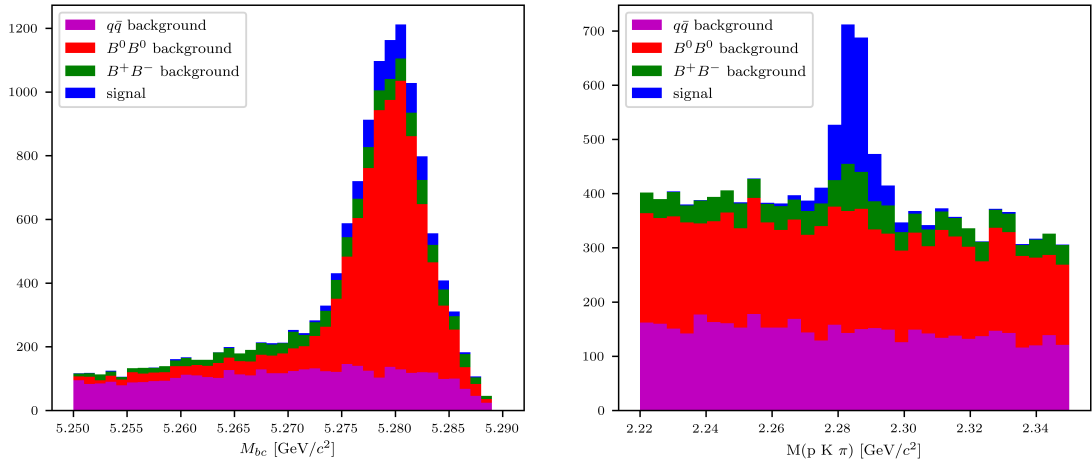


Figure (2.22) Distribution of M_{bc} (left) and invariant mass of neutral correlated Λ_c candidates (right), in the signal region after the above mentioned selection cuts.

2.4.4 $B^0 \rightarrow \Lambda_c^+ \text{ decays}$

Finally same procedure is applied also to the neutral anticorrelated decays. The final selections for the variables of *foxWolframR2*, *SignalProbability* and the momentum of the Λ_c candidates in the center of mass system:

- $\text{foxWolframR2} < 0.3$
- $\text{SignalProbability} > 0.15$
- $p_{CMS}^{\Lambda_c} < 1.4 \text{ GeV}/c$

Fig. 2.26 shows the M_{bc} and $M(pK\pi)$ distributions after applying these cuts.

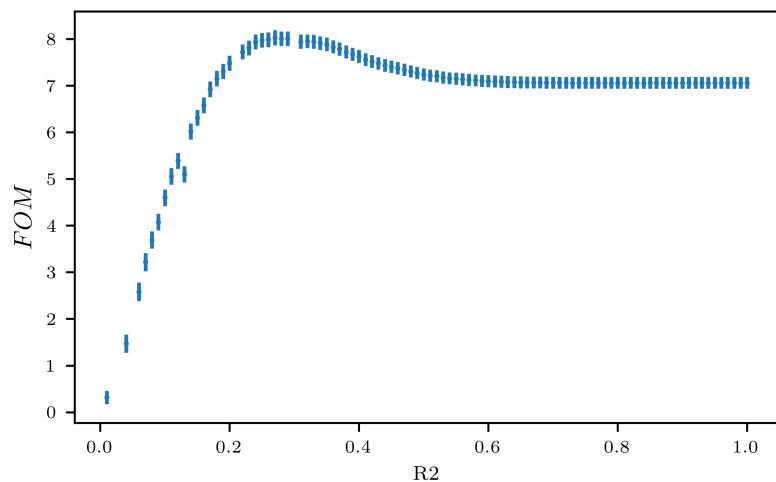


Figure (2.23) Figure of Merit values calculated at several cuts on the *foxWolframR2* variable

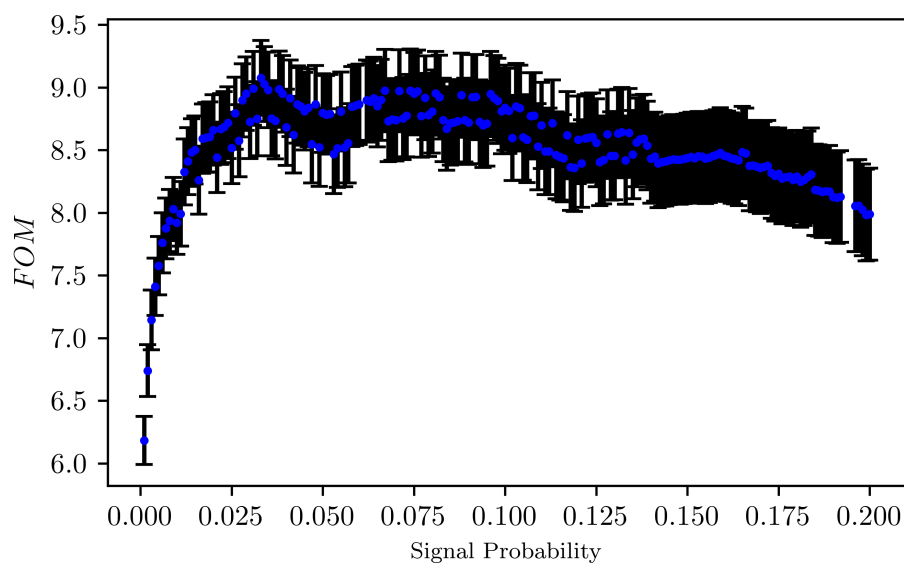


Figure (2.24) Figure of Merit values calculated at several cuts on the *SignalProbability* variable

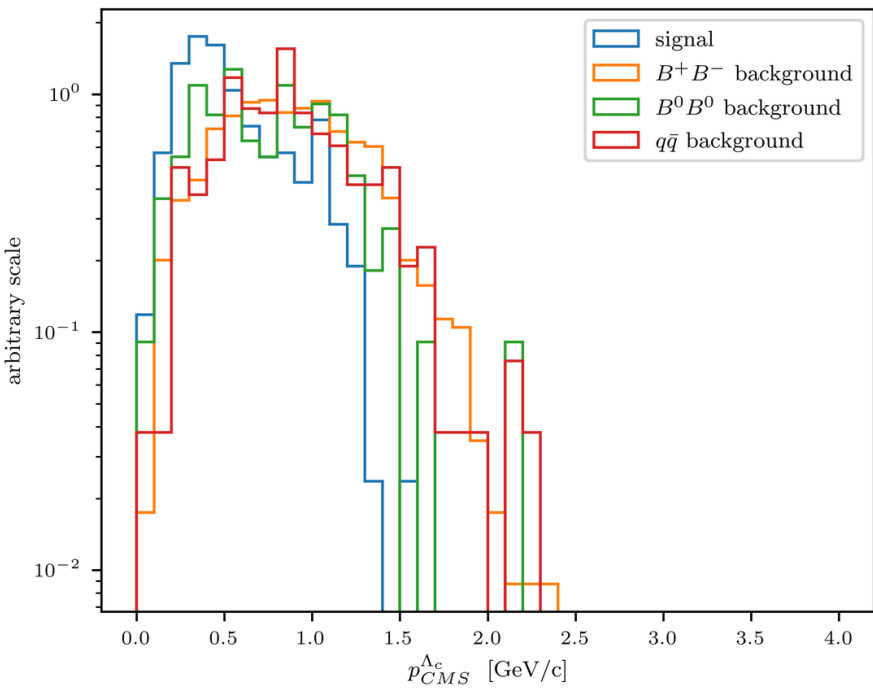


Figure (2.25) Distribution of Λ_c candidates momenta in the center of mass system

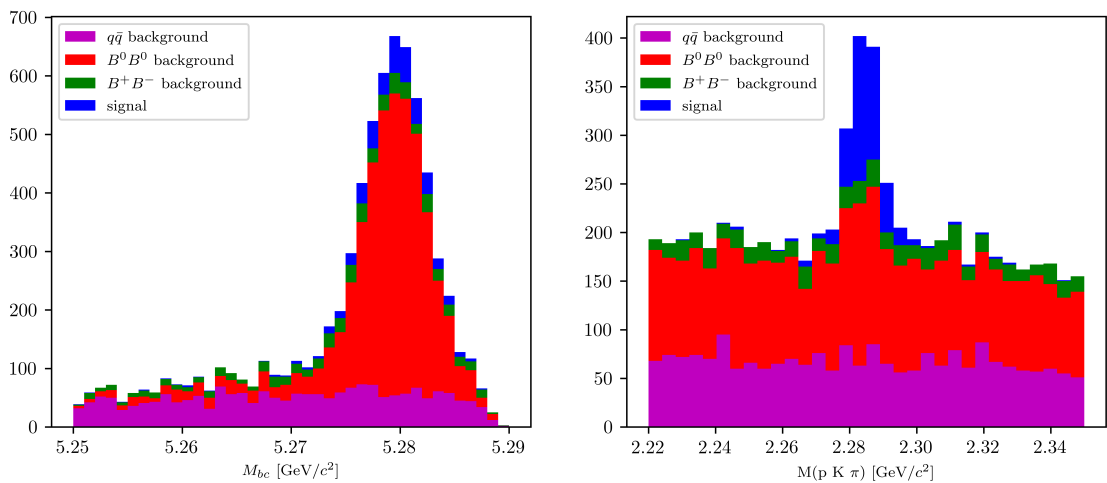


Figure (2.26) Distribution of M_{bc} (left) and invariant mass of neutral anticorrelated Λ_c candidates (right), in the signal region after the above mentioned selection cuts.

¹⁷⁷ Chapter 3

¹⁷⁸ 2D simultaneous fit

¹⁷⁹ 3.1 Probability Density Functions (PDFs) for the two ¹⁸⁰ dimensional fit

¹⁸¹ The reconstructed events can be categorized as follows:

- ¹⁸² • peaking in both M_{bc} and $M(pK\pi)$
- ¹⁸³ • peaking in M_{bc} but not in $M(pK\pi)$
- ¹⁸⁴ • peaking in $M(pK\pi)$ but not in M_{bc}
- ¹⁸⁵ • flat in both M_{bc} and $M(pK\pi)$

¹⁸⁶ The first category is represented by the reconstructed signal: signal events which are
¹⁸⁷ correctly reconstructed. The signal events which are misreconstructed fall into the third
¹⁸⁸ category. The sum of the two is the so called "total signal". The PDFs used to describe
¹⁸⁹ the total signal distributions are discussed first.

¹⁹⁰ 3.1.1 Total Signal fits

¹⁹¹ For all the decays, the final sample of total signal events presents a peak around the
¹⁹² expected B meson mass and a tail at low M_{bc} values.

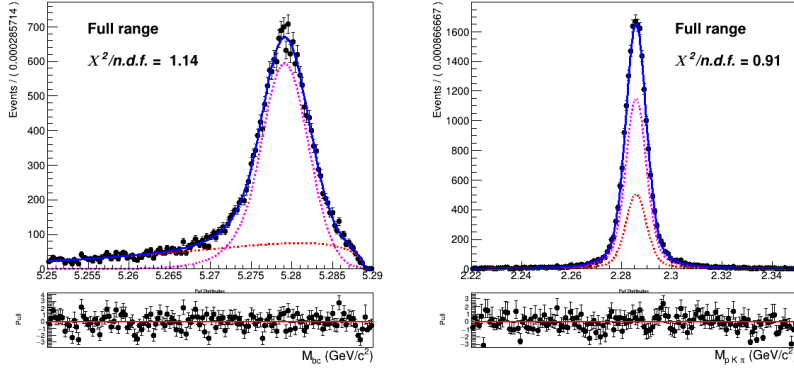


Figure (3.1) Two dimensional fit of charged correlated total signal events in M_{bc} and $M(pK\pi)$

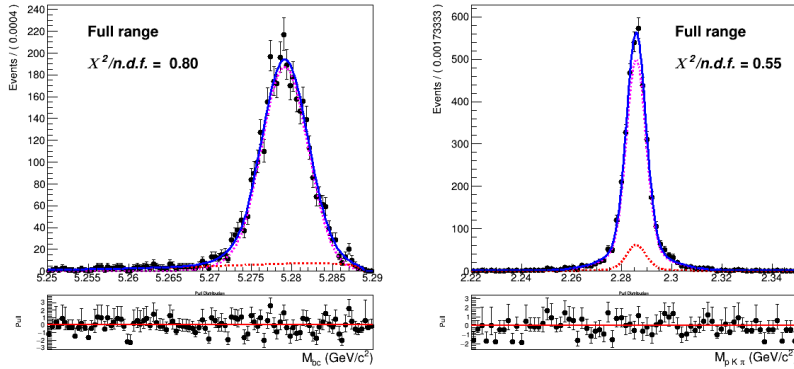


Figure (3.2) Two dimensional fit of charged anticorrelated total signal events in M_{bc} and $M(pK\pi)$

193 The 2D fits shown above are performed on five streams of signal MC with a sum of
 194 the following probability density functions:

$$P_{B,\Lambda_c}^{recSig}(M_{bc}, M(pK\pi)) = \Gamma_{CB}(M_{bc}) \times \rho_G(M(pK\pi)) \quad (3.1)$$

195 $P_{B,\Lambda_c}^{misSig}(M_{bc}, M(pK\pi)) = \Gamma_{ARG}(M_{bc}) \times \rho_G(M(pK\pi)) \quad (3.2)$

196 The first is used to fit the reconstructed signal and $\Gamma_{CB}(M_{bc})$ is a Crystal Ball function.
 197 The second is used to model the misreconstructed signal and $\Gamma_{ARG}(M_{bc})$ is an Argus
 198 function. In both cases a sum of three Gaussian functions $\rho_G(M(pK\pi))$ describes the
 199 mass of the Λ_c baryon.

200 As already said, only the events of reconstructed signal are considered as signal, while
 201 the misreconstructed signal is considered as background.

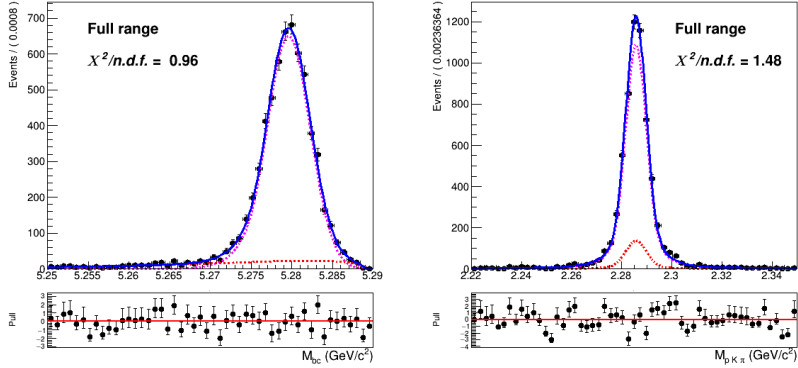


Figure (3.3) Two dimensional fit of neutral correlated total signal events in M_{bc} and $M(pK\pi)$

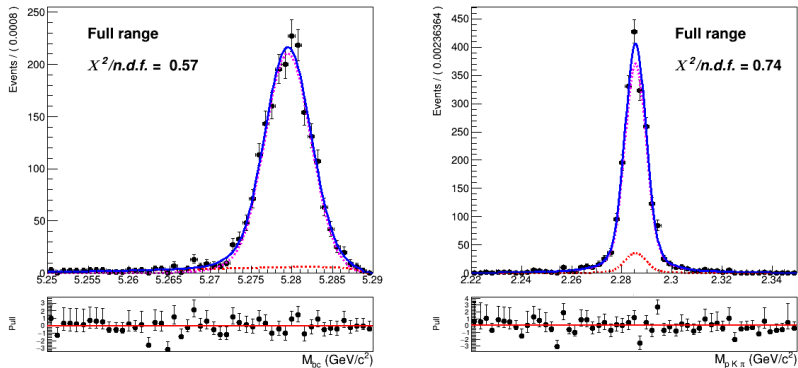


Figure (3.4) Two dimensional fit of neutral anticorrelated total signal events in M_{bc} and $M(pK\pi)$

3.1.2 M_{bc} peaking and flat background

The background composed of $B\bar{B}$ events where no Λ_c baryon is produced, is flat in its invariant mass, but can be distinguished in the following two categories:

- peaking in M_{bc} but not in $M(pK\pi)$
- flat in both M_{bc} and $M(pK\pi)$

as one can see in the following plots.

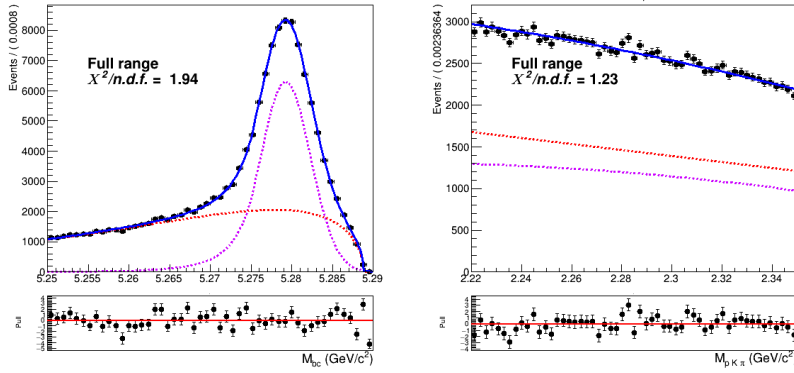


Figure (3.5) Two dimensional fit of charged correlated $B\bar{B}$ events in M_{bc} and $M(pK\pi)$

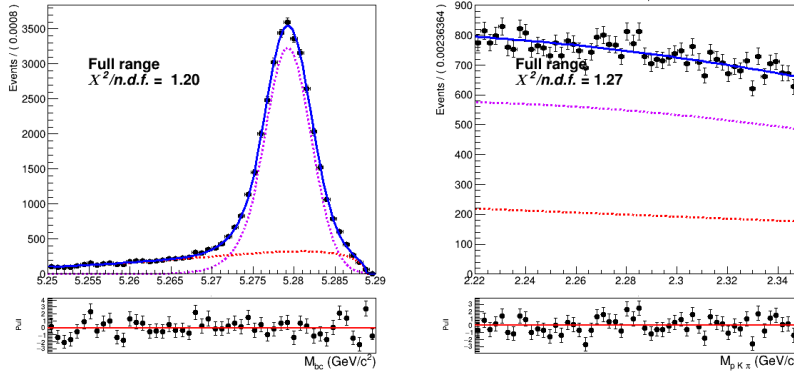


Figure (3.6) Two dimensional fit of charged anticorrelated $B\bar{B}$ events in M_{bc} and $M(pK\pi)$

209 This background presents a similar shape of the distribution in M_{bc} : the probability
210 density functions used for it are again a Crystal Ball and an Argus.

211 The two types of background (peaking/flat in M_{bc}) are described by:

$$P_{B,\Lambda_c}^{peaking}(M_{bc}, M(pK\pi)) = \Gamma_{CB}(M_{bc}) \times \rho_{Cheb(a_0,a_1)}(M(pK\pi)) \quad (3.3)$$

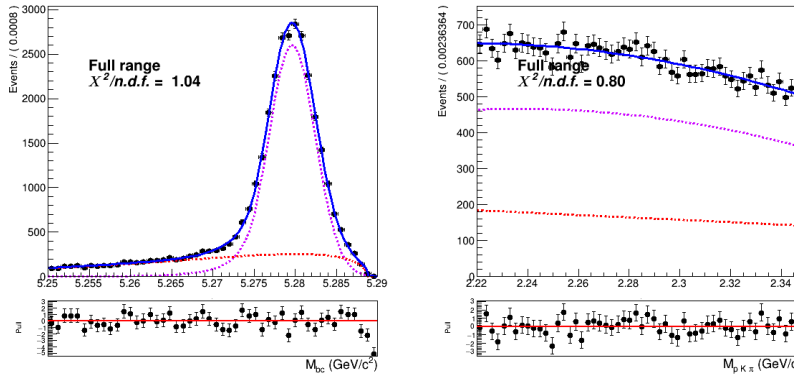


Figure (3.7) Two dimensional fit of neutral correlated $B\bar{B}$ events in M_{bc} and $M(pK\pi)$

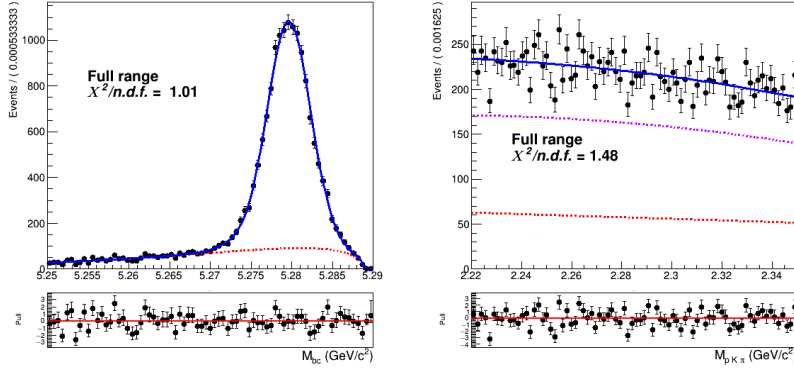


Figure (3.8) Two dimensional fit of neutral anticorrelated $B\bar{B}$ events in M_{bc} and $M(pK\pi)$

$$P_{B,\Lambda_c}^{flat}(M_{bc}, M(pK\pi)) = \Gamma_{ARG}(M_{bc}) \times \rho_{Cheb(b0)}(M(pK\pi)) \quad (3.4)$$

212
213 where $\rho_{Cheb(a0,a1)}(M(pK\pi))$ and $\rho_{Cheb(b0)}(M(pK\pi))$ represent a second order and first order
214 Chebychev polynomial function respectively.

215 3.1.3 Crossfeed background

216 The contamination of misreconstructed $B^0 \rightarrow \Lambda_c$ events in the B^+ signal (and vice-versa)
217 induces a background peaking in $M(pK\pi)$, but it also slightly peaks near the B meson
218 mass, as one can see in Fig. 3.9

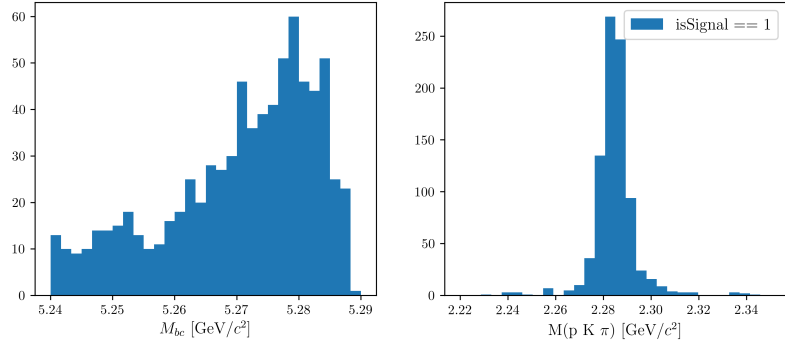


Figure (3.9) Crossfeed distribution in M_{bc} and $M(pK\pi)$

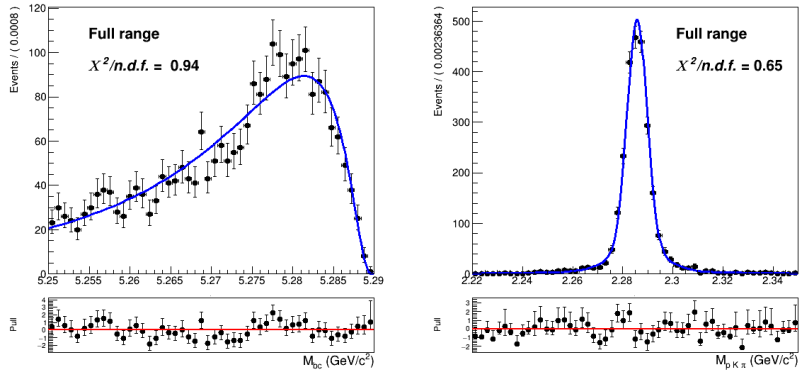


Figure (3.10) Two dimensional fit of crossfeed events in charged correlated channel in M_{bc} and $M(pK\pi)$

219 The 2D fit shown above are performed on five streams of signal MC with a sum of the

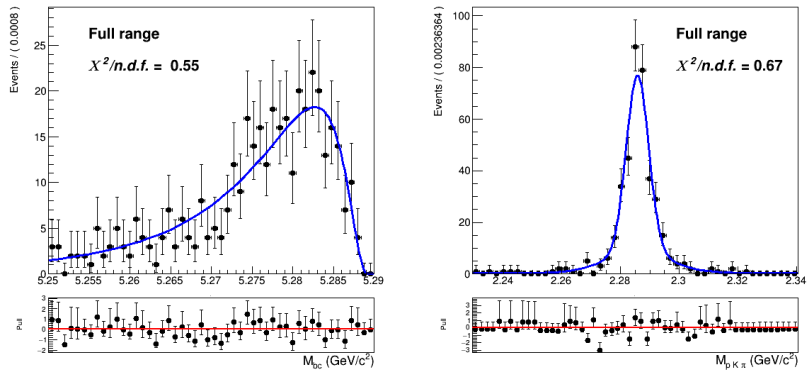


Figure (3.11) Two dimensional fit of crossfeed events in charged anticorrelated channel in M_{bc} and $M(pK\pi)$

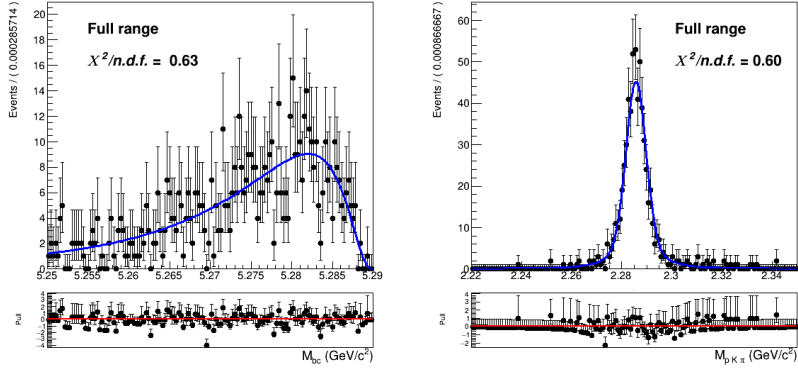


Figure (3.12) Two dimensional fit of crossfeed events in neutral correlated channel in M_{bc} and $M(pK\pi)$

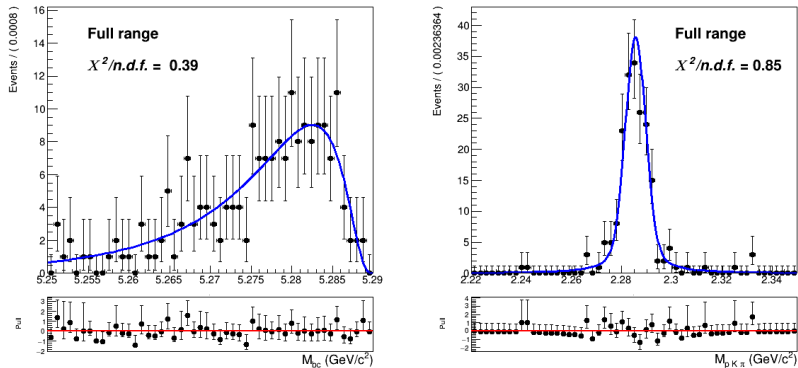


Figure (3.13) Two dimensional fit of crossfeed events in neutral anticorrelated channel in M_{bc} and $M(pK\pi)$

following probability density function:

$$P_{B,\Lambda_c}^{Crossfeed}(M_{bc}, M(pK\pi)) = \Gamma_{Novosibirsk}(M_{bc}) \times \rho_G(M(pK\pi)) \quad (3.5)$$

where $\Gamma_{Novosibirsk}(M_{bc})$ is a Novosibirsk function and the mass of the Λ_c baryon is described by the same sum of three Gaussian functions $\rho_G(M(pK\pi))$ as in Eq.3.1.

3.1.4 Continuum background

Besides the dataset recorded at the energy of the $\Upsilon(4S)$ resonance ($E_{CMS}^{on-res} = 10.58$ GeV), the *Belle* experiment recorded a sample of 89.4 fb^{-1} at an energy 60 MeV below the nominal $\Upsilon(4S)$ resonance ($E_{CMS}^{off-res} = 10.52$ GeV). The dataset allows to check for an appropriate modeling of the continuum MC simulation. Using the official tables (<https://belle.kek.jp/secured/nbb/nbb.html>) the off-resonance sample is scaled by

$$\frac{\mathcal{L}^{on-res}}{\mathcal{L}^{off-res}} \left(\frac{E_{CMS}^{off-res}}{E_{CMS}^{on-res}} \right)^2 \quad (3.6)$$

229 taking into account the difference in luminosity and in E_{CMS} (Energy in center of mass
230 system).

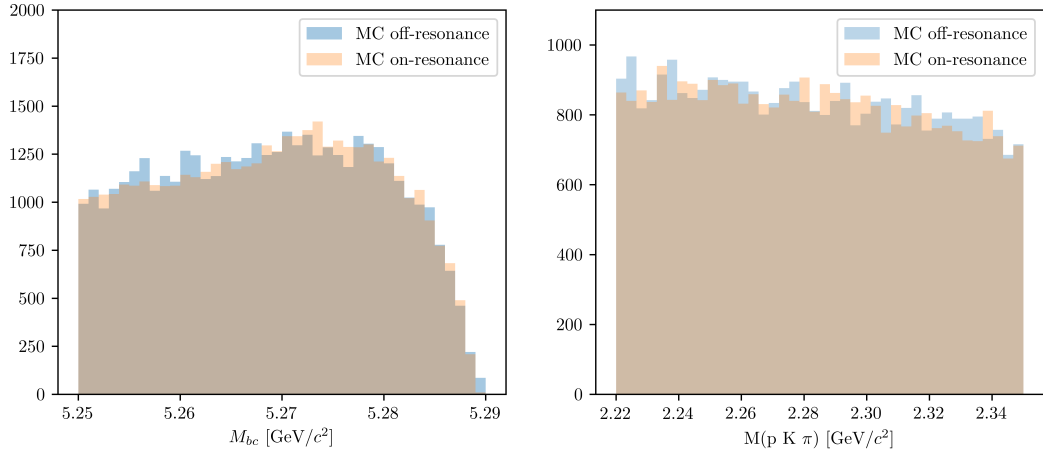


Figure (3.14) M_{bc} and $M(pK\pi)$ comparison between on-/off-resonance (scaled) Monte Carlo simulated continuum. The scaling is applied according to Eq. (3.6) and shifting the M_{bc} distribution by $E_{CMS}^{on-res} - E_{CMS}^{off-res}$.

231 The plot in Fig.3.14 shows the M_{bc} and $M(pK\pi)$ distributions in the MC on-/off-resonance
232 continuum after the scaling¹.

233 Ideally, provided that there's a good agreement between MC and data for the off-
234 resonance sample and also between the MC on-/off-resonance continuum after the scaling,
235 one could directly use the scaled off-resonance data to describe the continuum background
236 in the fit on data. There are two reasons that prevent this very straightforward approach:

- 237 • First, since the off-resonance MC (and data) present very low statistics (Fig. 3.15a
238 shows the Λ_c invariant mass in off-resonance data), scaling them with all the applied
239 selection cuts would cause the PDF describing the continuum to be very much
240 affected by statistical fluctuations.
- 241 • Secondly, the B meson candidates are reconstructed in both on-resonance and off-
242 resonance events for values of $M_{bc} \geq 5.22 \text{ GeV}/c^2$, but the E_{CMS} differs: there can be
243 effects of correlations between the applied *SignalProbability* cut and the M_{bc} variable
244 that one needs to take into account.

241¹it is obtained with the MC off-resonance sample being composed of 6 streams: the total amount is
242 normalized

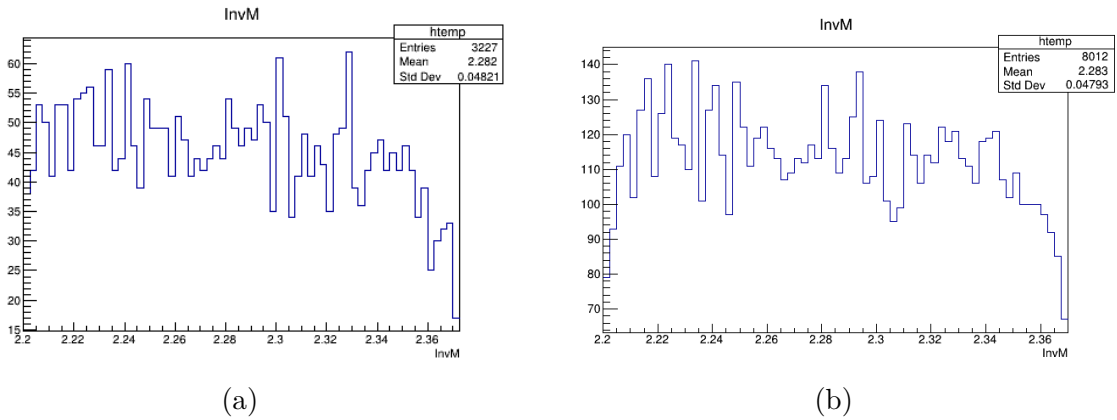


Figure (3.15) On the left: Λ_c invariant mass in off-resonance data (all nominal cuts applied). On the right: Λ_c invariant mass in off-resonance data after the continuum suppression cut removal.

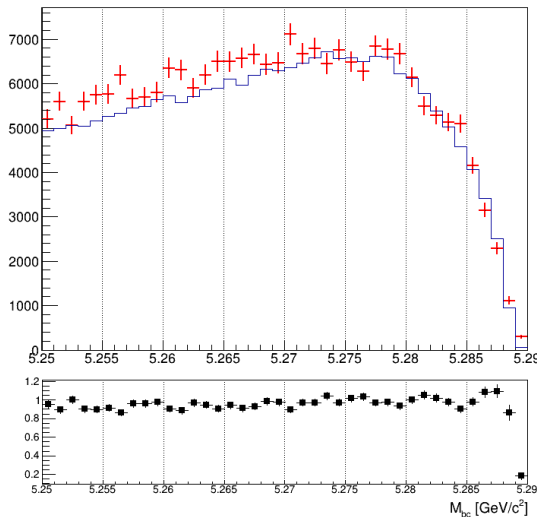


Figure (3.16) M_{bc} distributions of the MC (scaled) off-resonance sample (in red) and on-resonance (in blue) using 5 streams statistics and all nominal selection cuts applied.

245 In Fig. 3.16 one can notice some discrepancy in the shapes, apart from the not negligible
246 statistical fluctuations in the (scaled) off-resonance distribution.

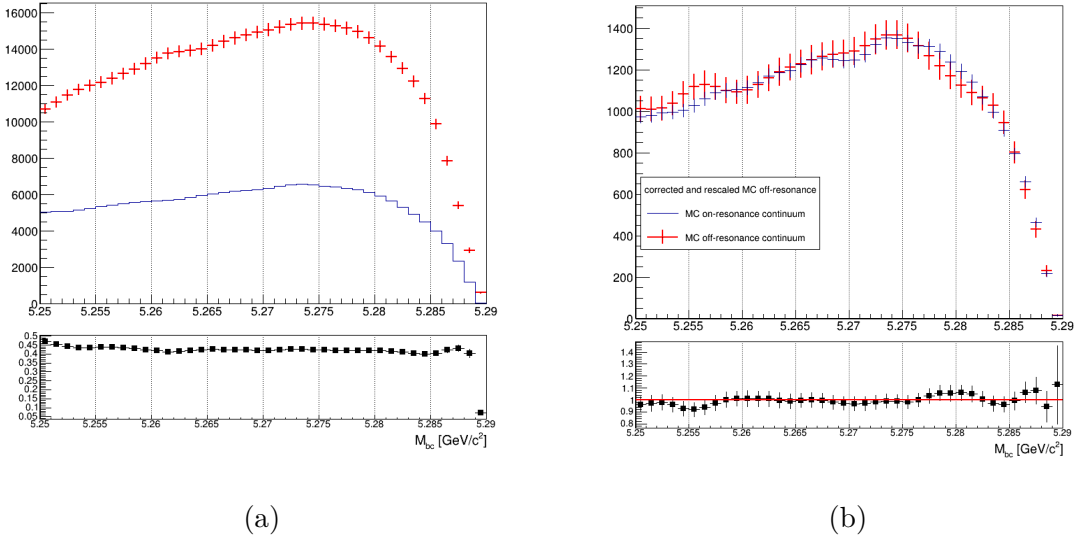
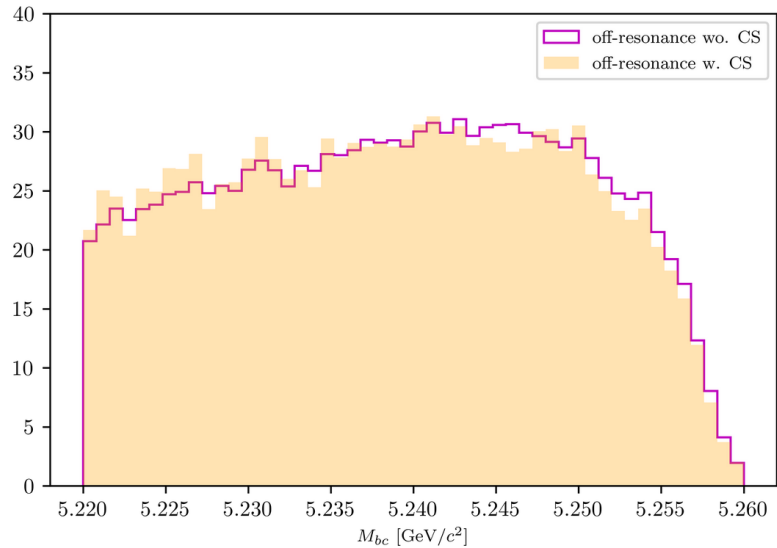


Figure (3.17) On the left: M_{bc} distributions of the MC off-resonance sample without continuum suppression and the MC continuum sample with applied continuum suppression. On the right: M_{bc} distributions of the corrected scaled MC off-resonance and on-resonance MC continuum.

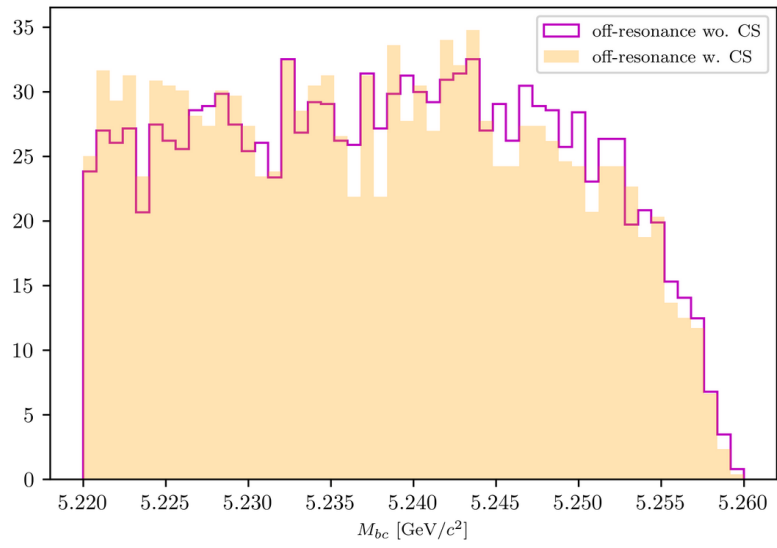
247 The procedure adopted to obtain the PDF describing the continuum background M_{bc}
248 distribution is the following:

- 249 • 5 streams of off-resonance MC were scaled according to Eq. (3.6) without continuum
250 suppression being applied and compared to the distribution of 5 streams of on-
251 resonance continuum
- 252 • From a ratio plot, like the one in Fig. 3.17a, the bin-correction is obtained to
253 correct the off-resonance data in the scaling procedure. To obtain the shape that
254 can describe the continuum background M_{bc} distribution on data the continuum
255 suppression is not applied on the off-resonance continuum sample, in order to acquire
256 more statistics.

257 This procedure is first tested on an independent MC sample (see Fig. 3.17b) to check the
258 result on simulated data before applying it on data.



(a)



(b)

Figure (3.18) Above: M_{bc} distributions of the MC off-resonance sample (5 streams) with and without continuum suppression. Below: M_{bc} distributions on data with and without continuum suppression.

- The validity of the method relies on the fact that the difference between on-/off-resonance continuum events are well modeled in MC and that the shape of the M_{bc} distribution doesn't change significantly when removing the continuum suppression cut both on MC and data (as one can see from Figures 3.18a - 3.18b). Additionally, the continuum suppression cut efficiency should be the same in data and MC in order to have the correct scaling on data with the above mentioned method. Fig.

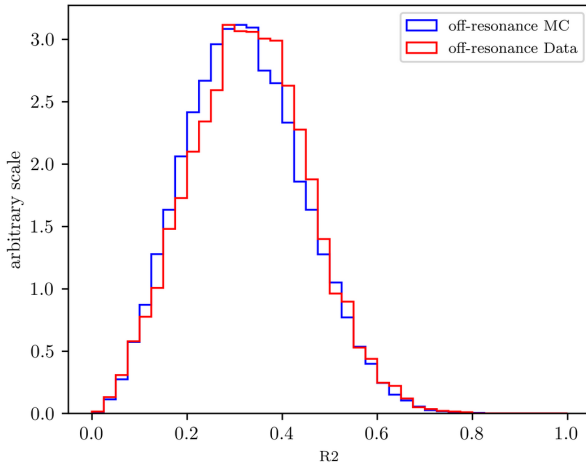


Figure (3.19) Distributions of variable *foxWolframR2* in off-resonance MC and data.

3.19 shows the distribution of the *foxWolframR2* variable in off-resonance MC and data. The slight shift visible in data can cause a different impact on data in terms of rejected continuum background when applying the $\text{foxWolframR2} < 0.3$ cut. It is found to reject about 60% of the continuum background in data, whereas it rejects 55% of the continuum background in MC (56% in on-resonance MC). Therefore in data one can expect about 2.25% less continuum background events. This discrepancy is not statistical significant (the statistical uncertainty for the continuum background events is of the level of $\sim 1\%$), a simple correction to the number of events can be applied on data and its possible systematics can be then taken into account.
The obtained distribution can be then fitted with a Novosibirsk function (see Fig. 3.20). This is the procedure which can be then applied on the off-resonance data to obtain the M_{bc} shape describing the continuum background in data.

In the Λ_c invariant mass one doesn't expect correlation effects, but nevertheless there can be differences due to the limited statistics of the off-resonance sample. In fact, in the case of on-resonance MC for the charged correlated decays some events in which Λ_c candidates survive nominal selection cuts are visible and can be described with a small Gaussian on the top of the flat background (Fig.3.21a). Due to the low statistics one cannot see a similar peak in the off-resonance sample (the Fig.3.21b shows a 5 streams statistics).

The shape describing the Λ_c invariant mass in the case of charged correlated decays is obtained from the simulated on-resonance continuum, again using 5 streams statistics (see Fig. 3.21a). In the other cases no peak is visible and therefore also the Λ_c invariant mass shape is obtained from 5 streams of off-resonance events.

Finally, it is possible to examine the validity of the whole procedure on the independent stream. Fig. 3.22 - 3.25 show the M_{bc} , $M(pK\pi)$ projections of the overlayed two dimensional PDFs obtained with the above described procedure.

The 2D PDF used for Fig. 3.22 can be written as:

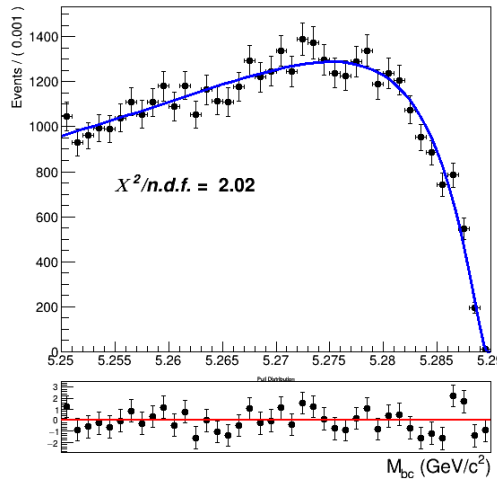


Figure (3.20) Fit of the M_{bc} distribution MC (scaled) off-resonance continuum (one stream).

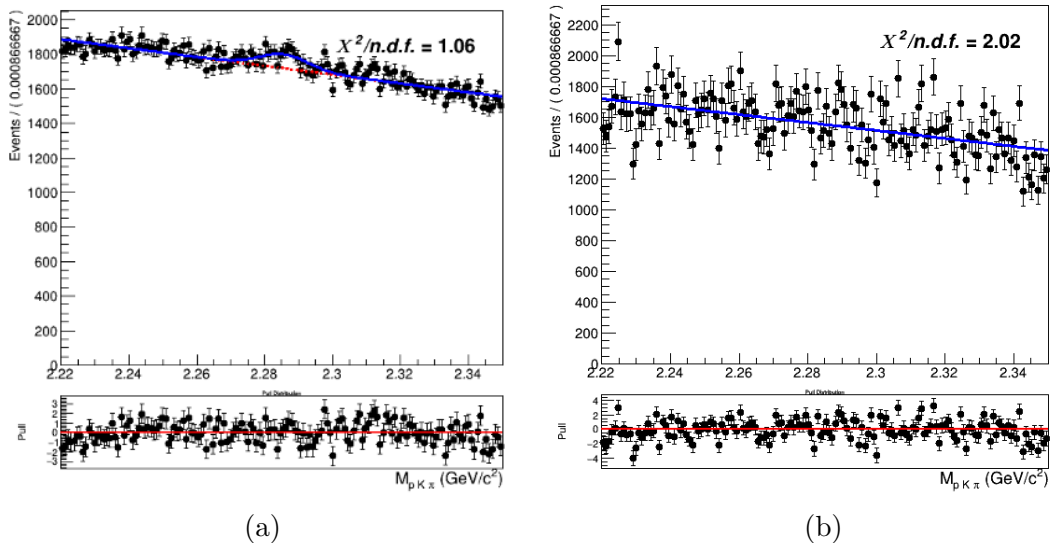


Figure (3.21) Comparison between 5 streams of MC on-resonance continuum 3.21a) and off-resonance (scaled) continuum in $M(pK\pi)$ (3.21b).

292

$$P_{B,\Lambda_c}^{Continuum}(M_{bc}, M(pK\pi)) = \Gamma_{Nov}(M_{bc}) \times [\rho_{Cheb1}(M(pK\pi)) + \rho_G(M(pK\pi))]$$

294

295 where, as already anticipated, the invariant mass is described by a sum of a first order
 296 Chebychev polynomial and the peak by the same triple Gaussian PDF adopted for the
 297 signal. The 2D PDF used for Fig. 3.23 and Fig. 3.24 differ only in the invariant mass, not
 298 having the triple gaussian. Whereas the 2D PDF used for Fig. 3.25 can be written as:

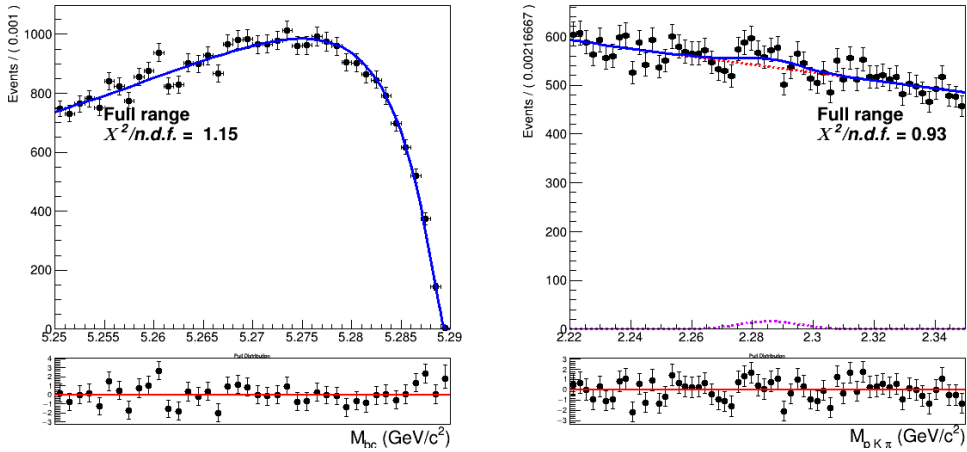


Figure (3.22) Two dimensional fit of charged correlated continuum events (one stream).

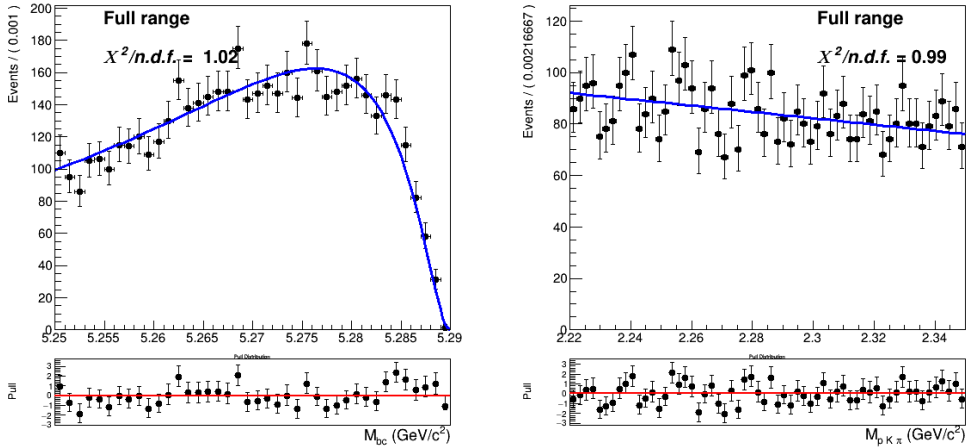


Figure (3.23) Two dimensional fit of charged anticorrelated continuum events (one stream).

299

$$300 \quad P_{B,\Lambda_c}^{Continuum}(M_{bc}, M(pK\pi)) = \Gamma_{Argus}(M_{bc}) \times [\rho_{Cheb1}(M(pK\pi)]$$

301

302 since the distribution in M_{bc} can be better described by an Argus.

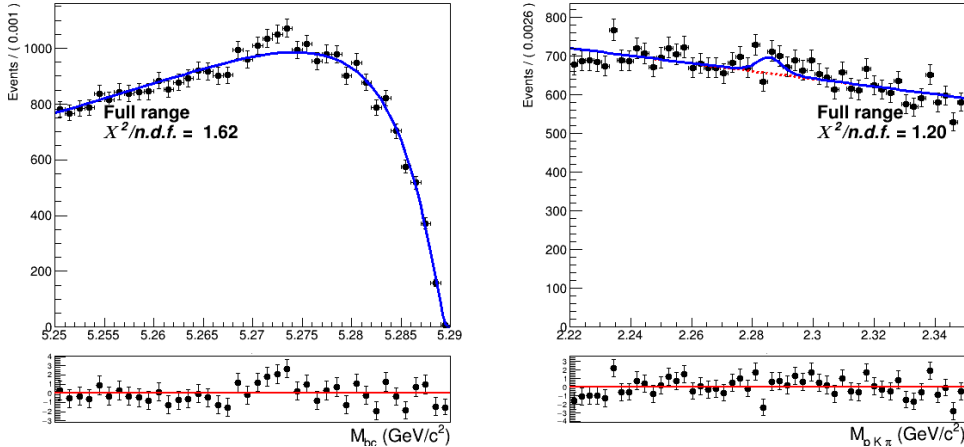


Figure (3.24) Two dimensional fit of continuum events (one stream).

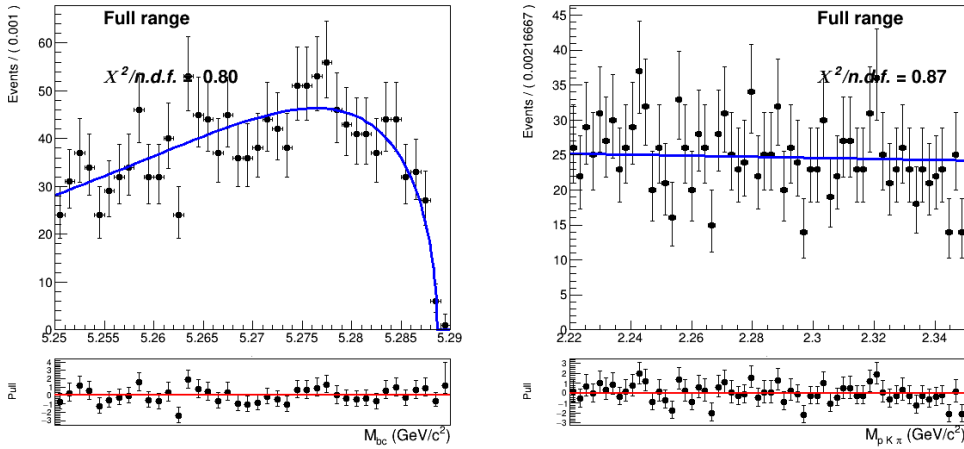


Figure (3.25) Two dimensional fit of continuum events (one stream).

3.2 Two dimensional fit on Monte Carlo

A total of six independent streams were used to construct/validate the fit model: each time five streams were used to construct the already discussed PDFs and the independent stream is used to test if the total PDF enables to extract the signal yield in an unbiased way (a total of six fits are performed on the six different streams of generic MC). To especially suppress the systematic uncertainties deriving from the amount of crossfeed the samples corresponding to the four different decay channels are fitted simultaneously. In all six fits all the shaping parameters are kept fixed, except:

- σ_{G1} : the width of the main of the three Gaussian functions in $\rho_G(M(pK\pi))$
- σ_{CB} parameter for the Crystal Ball describing the signal peak in M_{bc}

313 In the M_{bc} distribution the σ_{CB} width parameter for the Crystal Ball describing the M_{bc}
 314 peaking background is expressed as function of the signal σ_{CB} with a ratio fixed from MC.
 315 As for the normalizations, mis-/reconstructed signal events and M_{bc} peaking/flat back-
 316 ground events are floated in the two dimensional unbinned maximum likelihood fits.
 317 The continuum background normalization is kept fixed to the value obtained by the
 318 off-resonance scaling procedure.
 319 Instead, the normalization of crossfeed background events is determined by the fit in the
 320 following way:

$$N_{CrossBkg} = N_{recSig}^{corr} \cdot (\epsilon_{cross}/\epsilon_{recSig})^{corr} + N_{recSig}^{anticorr} \cdot (\epsilon_{cross}/\epsilon_{recSig})^{anticorr} \quad (3.7)$$

321 where N_{recSig}^{corr} ($N_{recSig}^{anticorr}$) are the fitted signal yields of the corresponding crossfeeding
 322 decay and $(\epsilon_{cross}/\epsilon_{recSig})$ are the ratios of misreconstruction efficiency and signal recon-
 323 struction efficiency as determined in the Monte Carlo. Since the crossfeed can likely
 324 occur both from correlated and anticorrelated channels, both are considered and summed
 325 together.

326 Exemplary, the distributions of stream 0 overlaid by the fitted PDF are depicted in
 327 Figs. 3.27 to 3.37. In Tables 3.1 to 3.4 the signal yields of the fits (**Reconstructed**
 328 **Signal**) to the two dimensional distributions for the six streams are listed and compared
 329 to the yields obtained from fits of signal distributions of each individual stream. The
 330 latter are the "expected" yields of reconstructed signal from a fit to the total signal events
 331 in the individual stream as the one plotted on Fig. 3.26 where all the parameters of the
 332 PDFs described in Eq. (3.1) are kept fixed and the corresponding yields are extracted from
 333 the fit. Note that in the case of Tables Table 3.3 - 3.4 the reconstructed signal yields are
 334 contaminated by events from the other neutral B^0 decay channel that experience mixing.
 335 Since those events cannot be analytically distinguished from the true signal events, the
 336 branching fraction calculation for neutral decays needs to take them into account and
 337 correct for their contribution (as will be shown in the next Chapter).

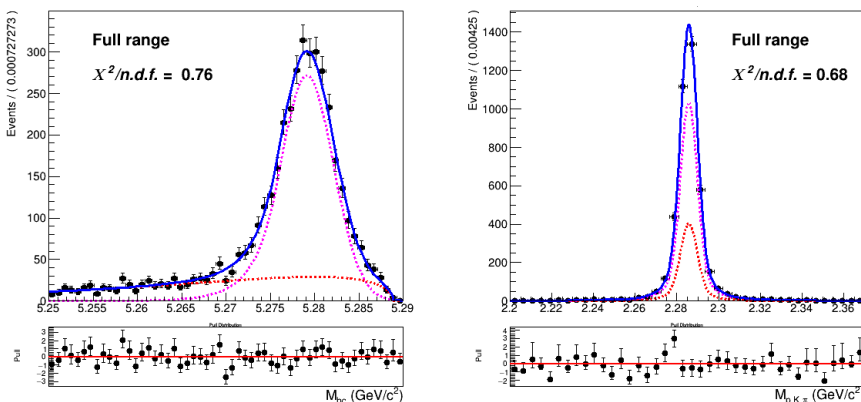


Figure (3.26) Two dimensional fit of Total Signal of stream 0 used to extract the expected reconstructed (corresponding to the PDF colored in magenta) and expected misreconstructed yields (corresponding to the PDF colored in red).

³³⁸ 3.2.1 Fit results for $B^- \rightarrow \Lambda_c^+ \text{ decays}$

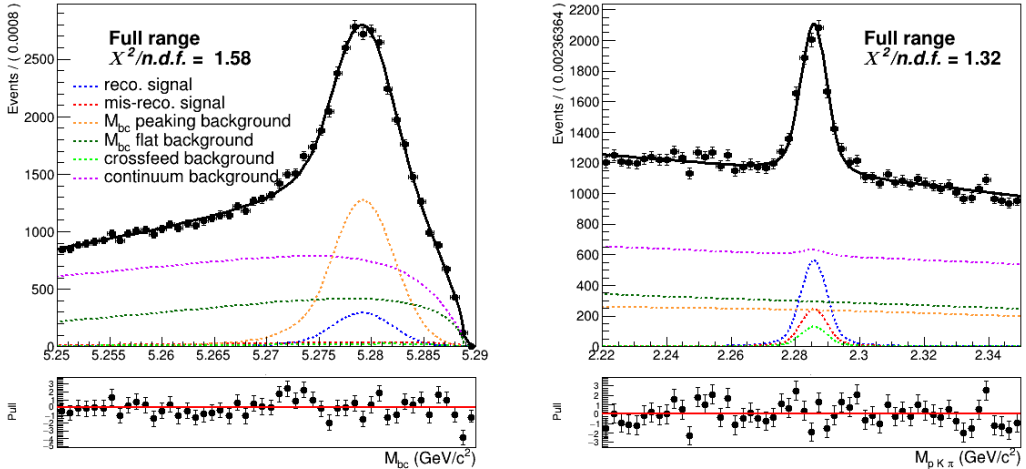


Figure (3.27) Projections of the two dimensional simultaneous fit on stream 0 Monte Carlo simulated data for charged correlated decays.

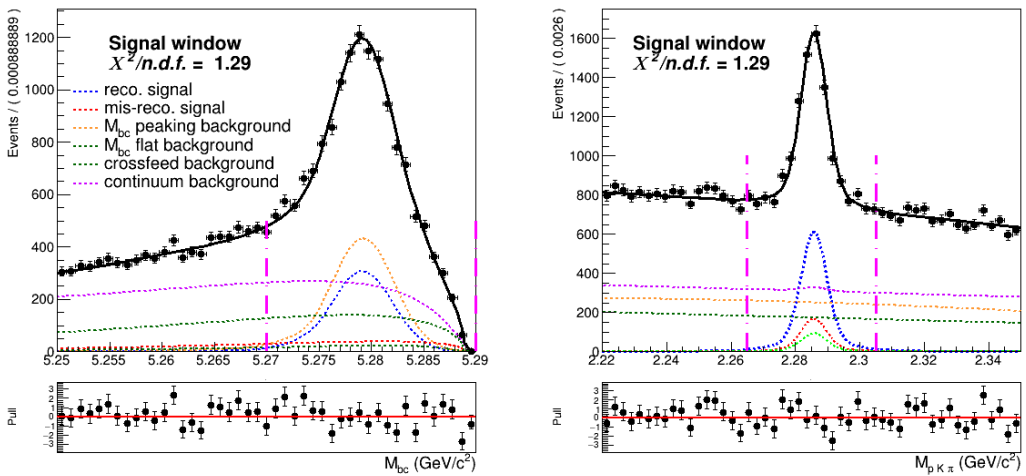


Figure (3.28) Projections of the two dimensional simultaneous fit on stream 0 Monte Carlo simulated data for charged correlated decays(in the signal window)

	Reconstructed Signal		Total Signal			
	fit	expected	fit	MC truth	fit - MC truth	
stream 0	2829 ± 130	2928 ± 66	4063 ± 157	4061	-2	-0.05%
stream 1	2811 ± 137	2956 ± 65	4095 ± 161	4084	11	0.3%
stream 2	2952 ± 141	2940 ± 65	4345 ± 165	4138	207	5.0%
stream 3	2747 ± 134	2867 ± 66	4267 ± 160	4105	162	3.9%
stream 4	3043 ± 138	3017 ± 67	4148 ± 157	4176	-28	-0.7%
stream 5	2818 ± 136	2816 ± 65	3999 ± 162	4001	-2	-0.05%
sum	17200	17524	24917	24565	348	1.4%

Table (3.1) Charged correlated decays: comparison of fitted and expected signal yields, fitted and truth-matched total signal for six streams of Belle generic MC when fitting the two dimensional distributions of M_{bc} and $M(pK\pi)$.

³³⁹ The yields obtained by the fit show a slight tendency of underestimation, but when
³⁴⁰ comparing the sums of them with the sum of expected values one can see the difference is
³⁴¹ within statistical fluctuations (within 2%).

³⁴² The tendency of underestimation is visible in , but it is just slightly larger than σ

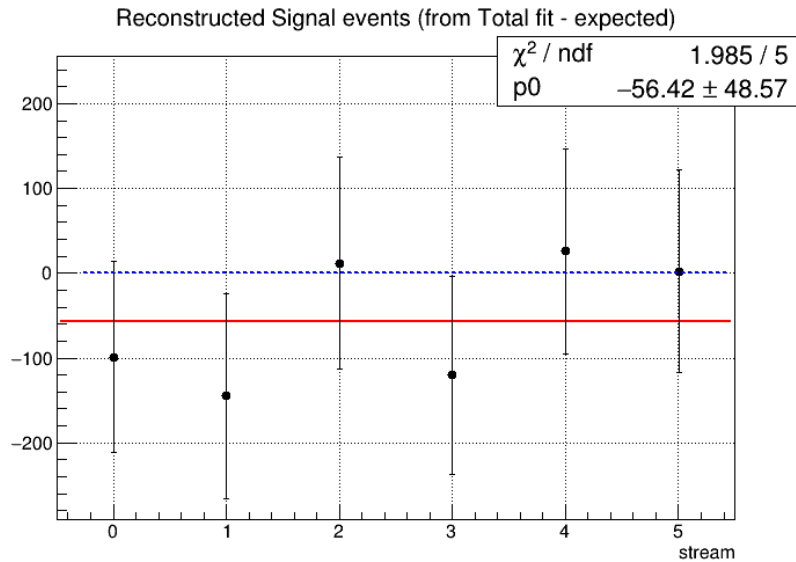


Figure (3.29) Residuals of signal yields (alias reconstructed signal, values reported in the first two columns of the above displayed table).

3.2.2 Fit results for $B^- \rightarrow \bar{\Lambda}_c^-$ decays

For the anticorrelated decays from charged B mesons the slight tendency is in the opposite direction. But the distribution of residuals (see Fig. 3.30) shows this slight overestimation is well within the statistical uncertainty.

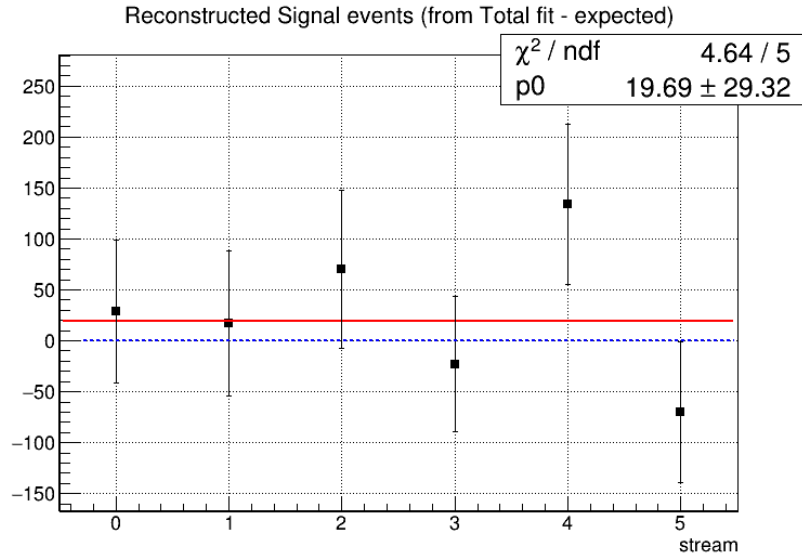


Figure (3.30) Residuals of signal yields (alias reconstructed signal, values reported in the first two columns of the above displayed table).

	Reconstructed Signal		Total Signal			fit - MC truth
	fit	expected	fit	MC truth	fit - MC truth	
stream 0	724 ± 64	695 ± 28	813 ± 73	765	48	6.3%
stream 1	726 ± 65	709 ± 29	802 ± 67	785	17	2.2%
stream 2	788 ± 72	718 ± 29	911 ± 72	797	114	14.3%
stream 3	679 ± 60	702 ± 29	768 ± 66	802	-34	4.2%
stream 4	844 ± 73	710 ± 29	982 ± 73	785	197	25.1%
stream 5	605 ± 63	675 ± 29	722 ± 63	760	-38	-5.0%
sum	4366	4209	4998	4694	304	6.5%

Table (3.2) Charged anticorrelated decays: comparison of fitted and expected signal yields, fitted and truth-matched total signal for six streams of Belle generic MC when fitting the two dimensional distributions of M_{bc} and $M(pK\pi)$.

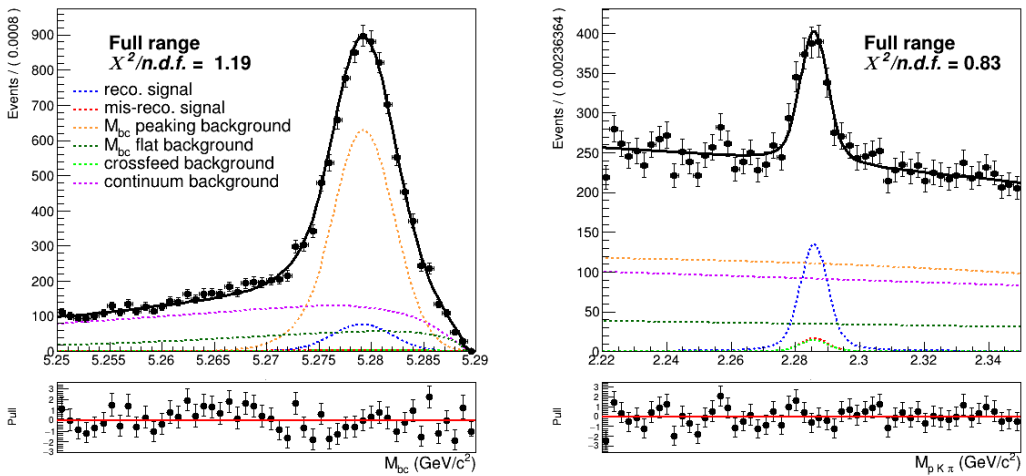


Figure (3.31) Projections of the two dimensional simultaneous fit on stream 0 Monte Carlo simulated data for charged anticorrelated decays.

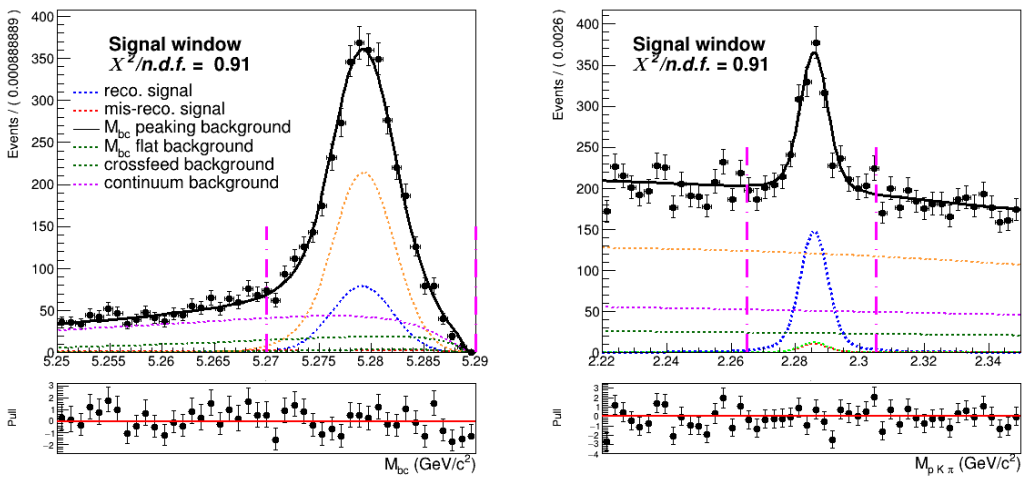


Figure (3.32) Projections of the two dimensional simultaneous fit on stream 0 Monte Carlo simulated data for charged anticorrelated decays (in the signal window).

³⁴⁷ 3.2.3 Fit results for $\bar{B}^0 \rightarrow \Lambda_c^+ \text{ decays}$

³⁴⁸ Also in the case of the neutral correlated one can observe a slight overestimation in the
³⁴⁹ reconstructed signal yields. The residuals (see Fig. 3.33) show that this is not so negligible:
³⁵⁰ the significance is about 1.5σ .

	Reconstructed Signal		Total Signal			
	fit	expected	fit	MC truth	fit - MC truth	
stream 0	1329 ± 69	1240 ± 38	1390 ± 70	1379	11	0.8%
stream 1	1314 ± 68	1327 ± 38	1319 ± 66	1287	14	2.5%
stream 2	1266 ± 68	1254 ± 38	1273 ± 65	1251	22	1.8%
stream 3	1320 ± 67	1248 ± 38	1316 ± 66	1255	35	4.9%
stream 4	1227 ± 67	1214 ± 38	1300 ± 66	1223	77	6.3%
stream 5	1282 ± 70	1233 ± 38	1251 ± 66	1246	5	0.4%
sum	7738	7516	7709	7525	140	1.86%

Table (3.3) Comparison of fitted and expected signal yields, fitted and truth-matched total signal for six streams of Belle generic MC when fitting the two dimensional distributions of M_{bc} and $M(pK\pi)$.

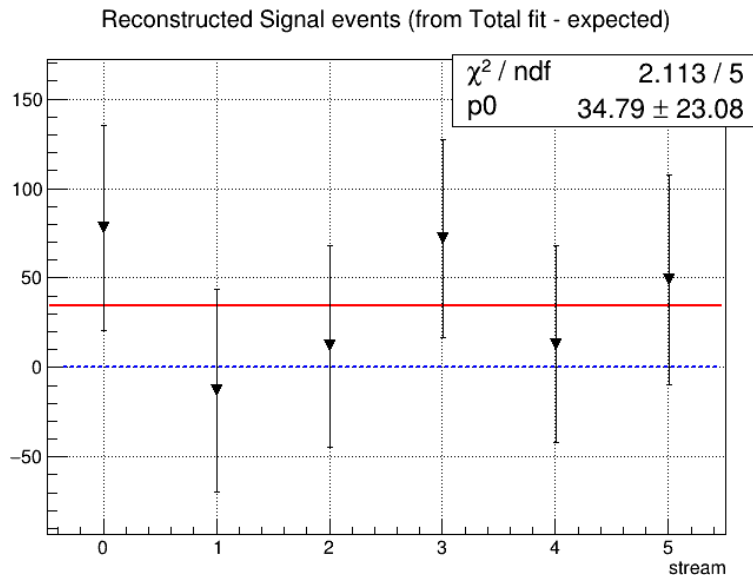


Figure (3.33) Residuals of signal yields for neutral correlated decays.

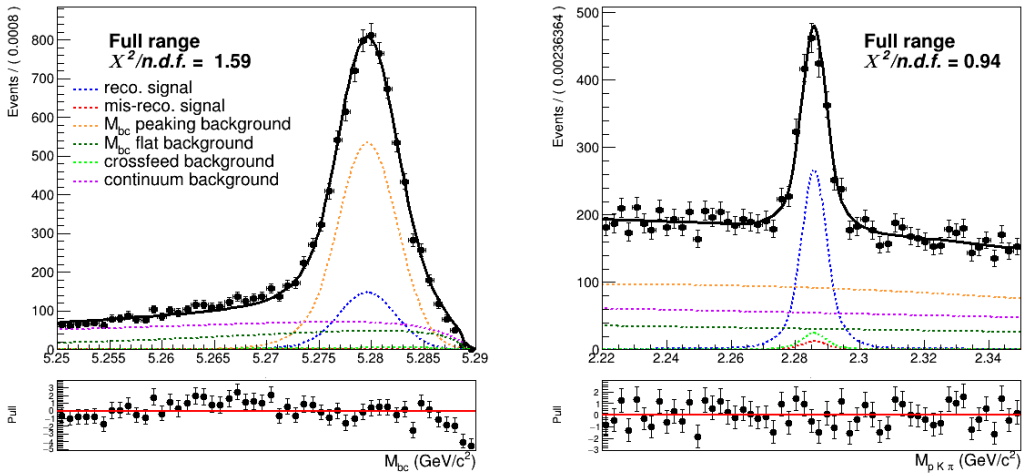


Figure (3.34) Projections of the two dimensional simultaneous fit on stream 0 Monte Carlo simulated data for neutral correlated decays.

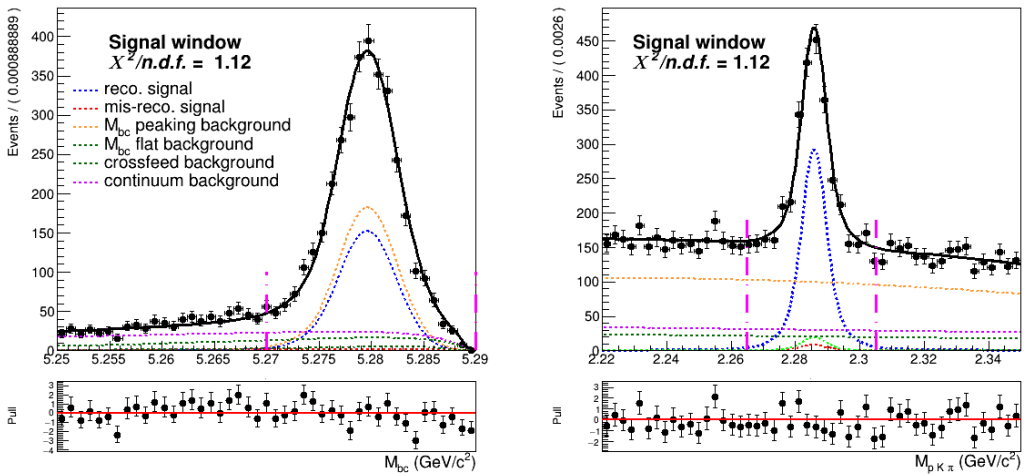


Figure (3.35) Projections of the two dimensional simultaneous fit on stream 0 Monte Carlo simulated data for neutral correlated decays.

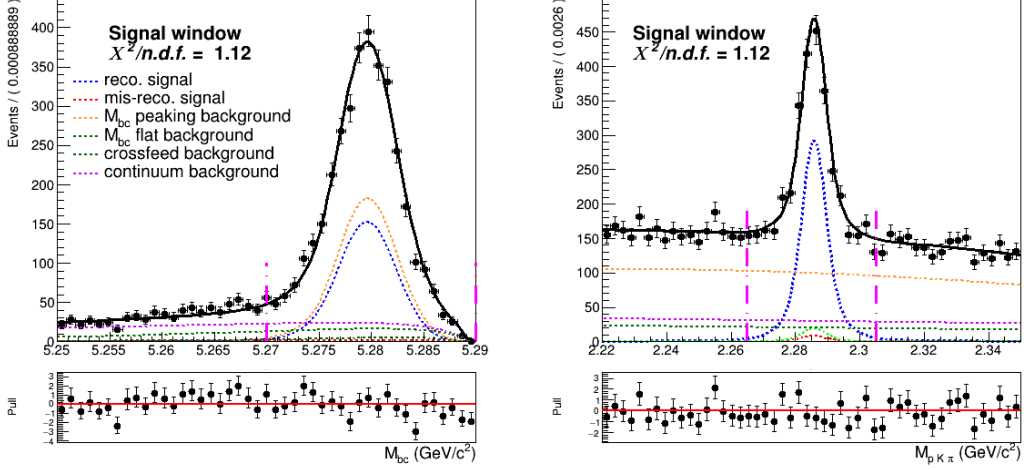


Figure (3.36) Projections of the two dimensional simultaneous fit on stream 0 Monte Carlo simulated data for neutral correlated decays (in the signal window).

³⁵¹ 3.2.4 Fit results for $\bar{B}^0 \rightarrow \bar{\Lambda}_c^-$ decays

	Reconstructed Signal		Total Signal			
	fit	expected	fit	MC truth	fit - MC truth	
stream 0	567 ± 45	575 ± 29	657 ± 45	668	-11	-1.6%
stream 1	565 ± 46	607 ± 21	660 ± 47	687	-27	-3.9%
stream 2	574 ± 46	593 ± 20	659 ± 45	639	20	3.1%
stream 3	714 ± 49	596 ± 21	792 ± 52	680	112	16.4%
stream 4	603 ± 50	594 ± 21	693 ± 50	638	55	8.6%
stream 5	589 ± 63	595 ± 21	603 ± 44	624	-21	3.4%
sum	3612	3560	4064	3936	170	4.3%

Table (3.4) Neutral anticorrelated decays: comparison of fitted and expected signal yields, fitted and truth-matched total signal for six streams of Belle generic MC when fitting the two dimensional distributions of M_{bc} and $M(pK\pi)$.

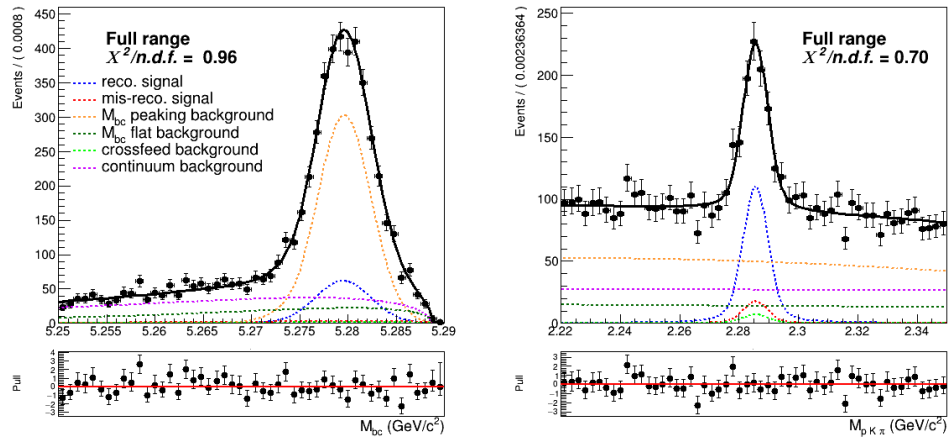


Figure (3.37) Projections of the two dimensional simultaneous fit on stream 0 Monte Carlo simulated data for neutral anticorrelated decays.

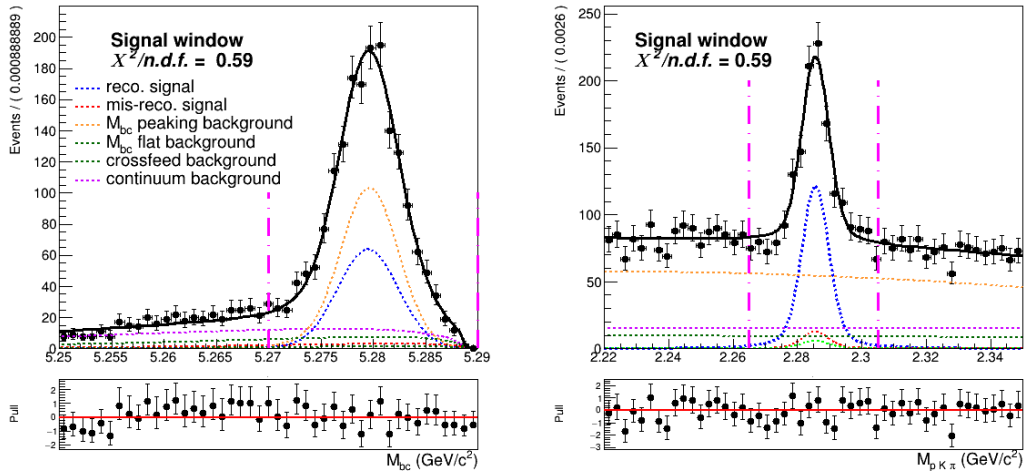


Figure (3.38) Projections of the two dimensional simultaneous fit on stream 0 Monte Carlo simulated data for neutral anticorrelated decays (in the signal window).

3.2.5 Fit residuals

Fig. 3.39 shows the residuals in each fit (stream by stream), calculated as the difference of reconstructed signal yield in the two dimensional fit from the expected value (in the fit of the total signal events). Since the signal events are the same in the two fits, the resulting yields are correlated. Therefore the uncertainties on the residuals are calculated (on a first approximation) as:

$$\sigma_{res} = \sqrt{(\sigma_{tot}^2 - \sigma_{sig}^2)} \quad (3.8)$$

Some of the results may seem not well distributed around 0.

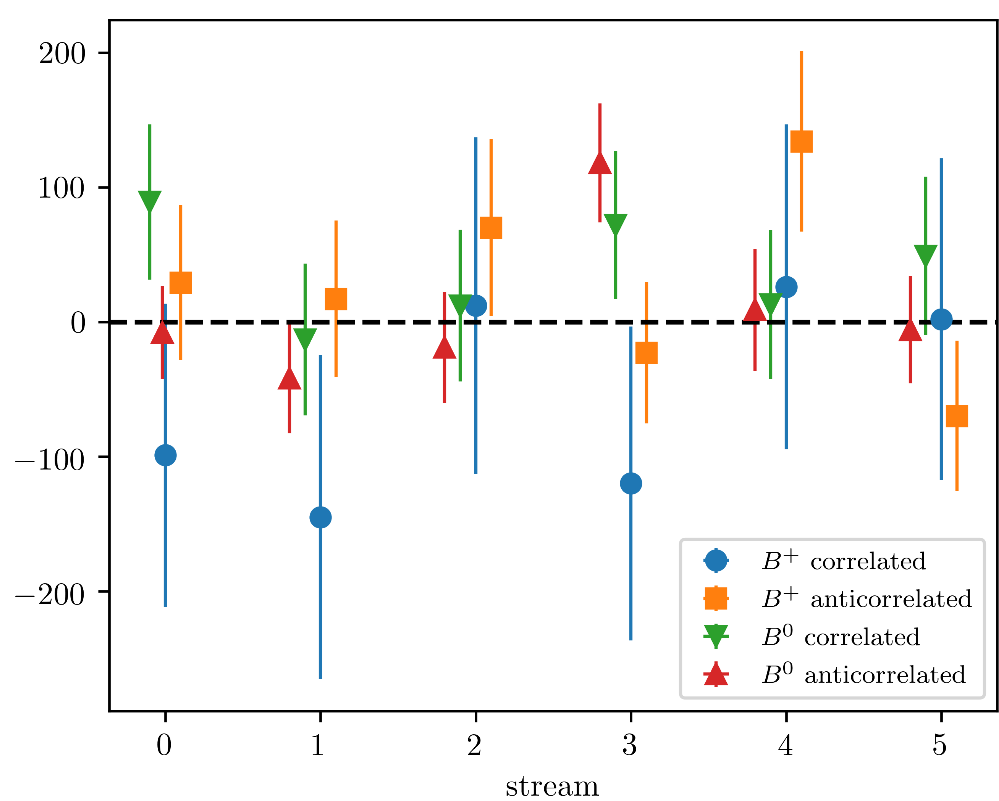


Figure (3.39) Residuals of the fitted signal yields resulting from the simultaneous 2D fit by stream and decay mode.

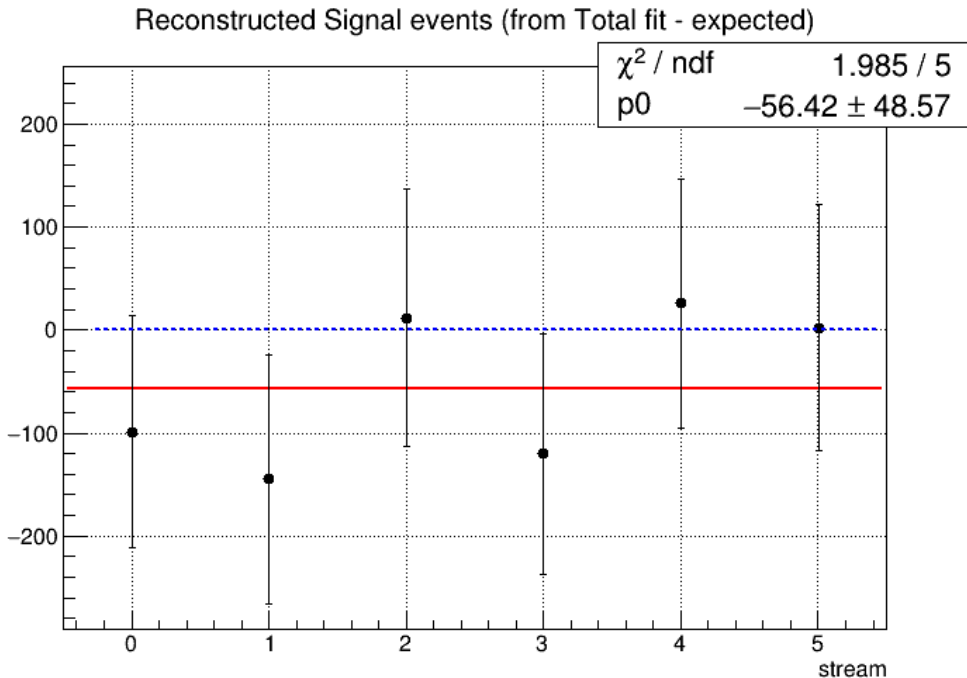


Figure (3.40) Residuals of the fitted signal yields of charged correlated decays.

359 3.2.6 toy Monte Carlo study

360 For the fit model also toy MC pseudo-experiments were performed in order to confirm
 361 the behavior of the fit setup. With toy MC experiments the yields, errors and the pulls
 362 of the fit are studied by generating our own pseudo-datasets, according to the MC (see
 363 plots in 3×10^3 pseudo-datasets are constructed, where each dataset was generated with
 364 the expected amount of events, distributed according to the Poisson distribution. Then
 365 the composition of each toy pseudo-experiment is fitted as if they were data, and the
 366 pull-value distributions of the fit results are calculated. From the plots showing the pull
 367 distributions of the fitted signal yields one can conclude that no bias is present.

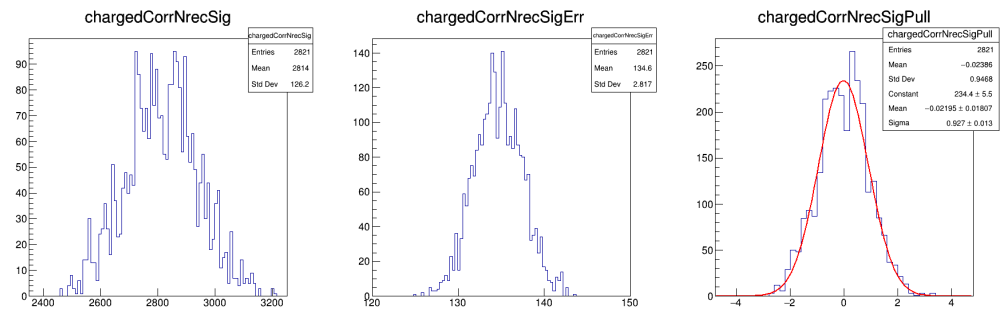


Figure (3.41) Plots showing distributions of the fitted signal yields, errors and the pull distribution of all pseudo-fits for the charged correlated decays.

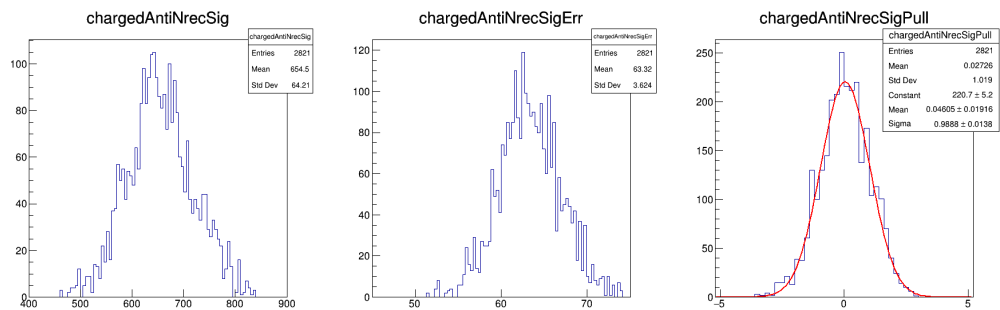


Figure (3.42) Plots showing distributions of the fitted signal yields, errors and the pull distribution of all pseudo-fits for the charged anticorrelated decays.

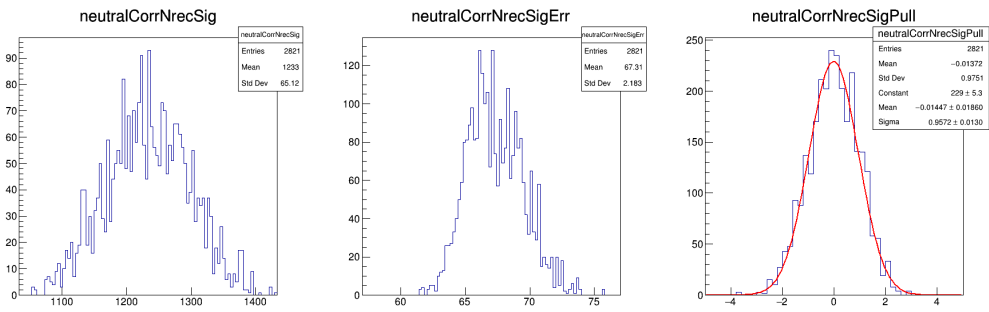


Figure (3.43) Plots showing distributions of the fitted signal yields, errors and the pull distribution of all pseudo-fits for the neutral correlated decays.

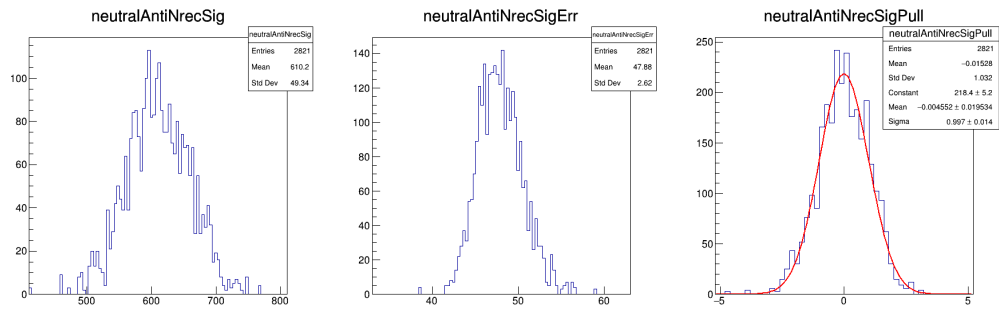


Figure (3.44) Plots showing distributions of the fitted signal yields, errors and the pull distribution of all pseudo-fits for the neutral anticorrelated decays.

368

Chapter 4

369

B_{tag} fit

- 370 The normalization for the branching fractions is determined from the number of correctly
371 tagged B mesons. This value is again determined by fitting the M_{bc} distribution of all B
372 meson candidates tagged by FEI regardless of the signal side B meson decay.
373 The tagged B meson candidates are selected according to the selection criteria used for
374 the M_{bc} variable already illustrated in subsections Secs. 2.4.1 to 2.4.4.

375

4.1 Probability Density Functions (PDFs) for the B_{tag}

376 The reconstructed events can be categorized as follows:

- 377 • correctly reconstructed B meson candidates: **reconstructed signal**
378 • misreconstructed B meson candidates: **misreconstructed signal**
379 • B^0 mesons misreconstructed as B^+ (and vice-versa): **crossfed background**
380 • and **continuum background**

381

4.1.1 Total Signal fits

382 As in the 2D fits the total signal is distinguished in **reconstructed** and **misreconstructed**
383 **signal** depending on whether it's peaking or not in M_{bc} .
384 Fig. 4.1 shows the fit on tagged charged B mesons corresponding to the normalization
385 for the branching fractions of $B^- \rightarrow \Lambda_c^+$ decays. The M_{bc} distribution of the tagged B
386 mesons is fitted with a combination of Crystal Ball and Gaussian as for the "peaking"
387 component and the "flat" component is fitted with a Novosibirsk function. For the other
388 decay channels instead an Argus function is used to describe the misreconstructed signal
389 (see Figs. 4.2 to 4.4).

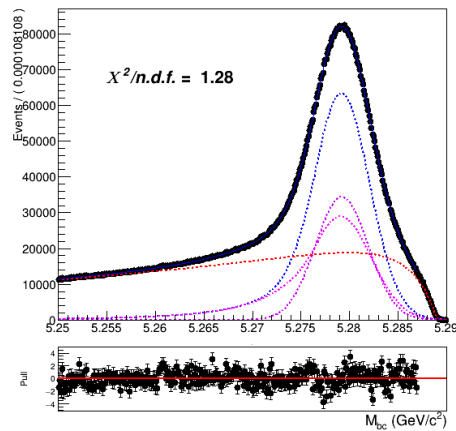


Figure (4.1) Fitted distribution of tagged charged B mesons in the charged correlated decays sample: reconstructed signal events are described by the blue dotted PDF, the misreconstructed with a Novosibirsk function (red dotted).

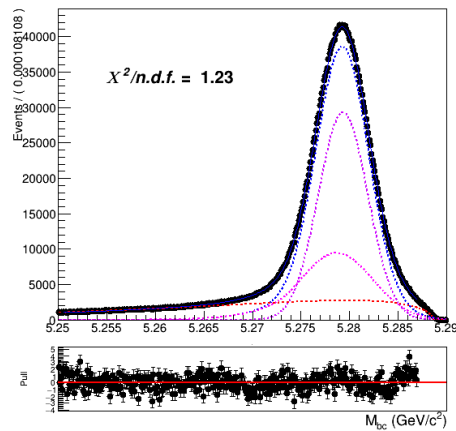


Figure (4.2) Fitted distribution of tagged charged B mesons in the charged anticorrelated decays sample.

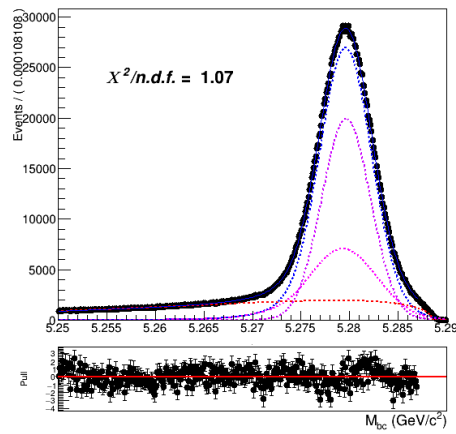


Figure (4.3) Fitted distribution of tagged neutral B mesons reconstructed in neutral correlated decays.

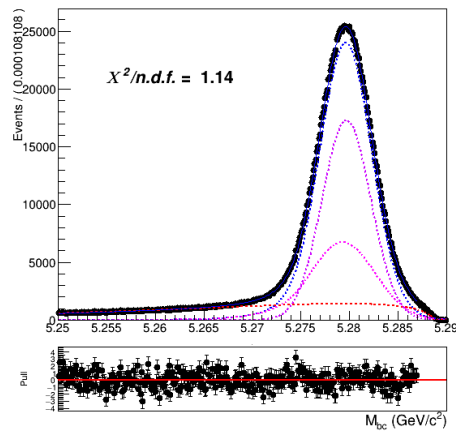


Figure (4.4) Fitted distribution of tagged charged B mesons reconstructed in neutral anticorrelated decays.

390 4.1.2 Crossfeed PDF

391 The crossfeed background is always fitted instead with a sum of a Novosibirsk and an
 392 asymmetric Gaussian PDF.

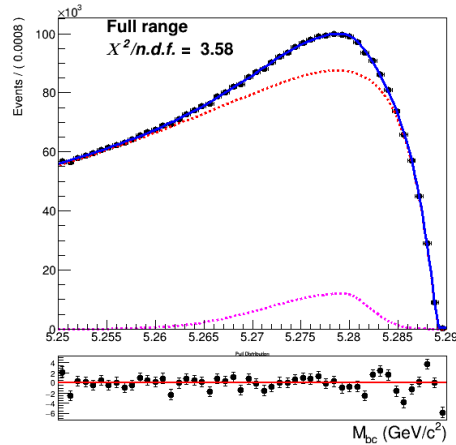


Figure (4.5) Crossfeed distribution of charged correlated decays fitted with a sum of Novosibirsk (red) and asymmetric Gaussian PDF (magenta)

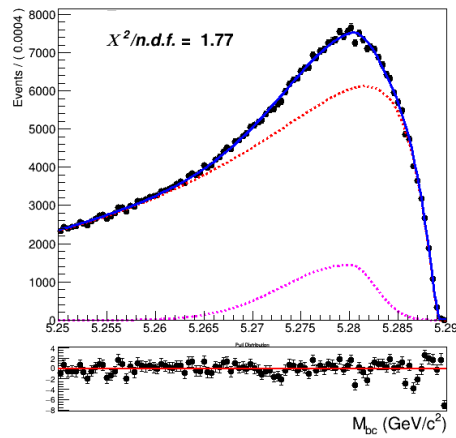


Figure (4.6) Crossfeed distribution of charged anticorrelated decays

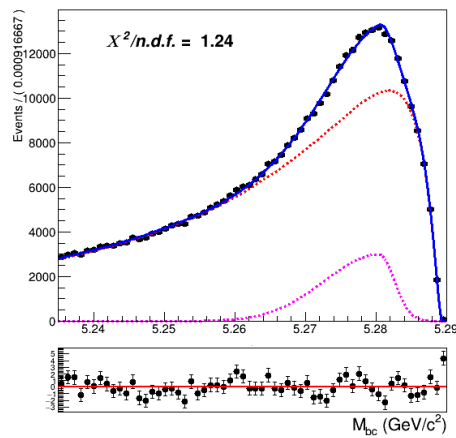


Figure (4.7) Crossfeed distribution of neutral correlated decays

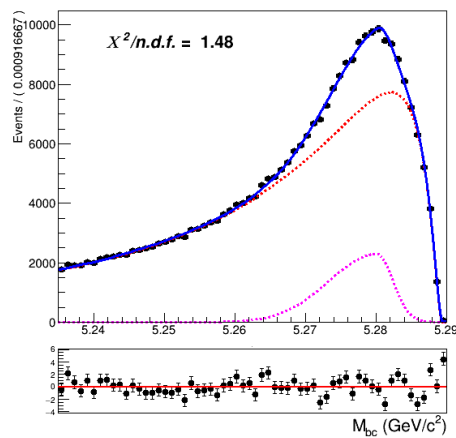


Figure (4.8) Crossfeed distribution of neutral anticorrelated decays

393 **4.1.3 Continuum PDF**

394 As for the continuum background, a similar procedure as the one described already for the
 395 two dimensional fit was adopted:

- 396
- first the off-resonance sample is scaled accordingly

397

 - the ratio between the scaled off-resonance and the on-resonance in MC is calculated
 398 in each bin (see Fig.4.9a)

399

 - the bin-correction is applied on an independent stream and the scaled and bin-
 400 corrected M_{bc} distribution is compared with the on-resonance distribution as shown
 401 in Fig.4.9b

402 Being the statistics much larger than in the 2D sample, there's no need to remove the
 403 continuum suppression cut on the off-resonance sample.

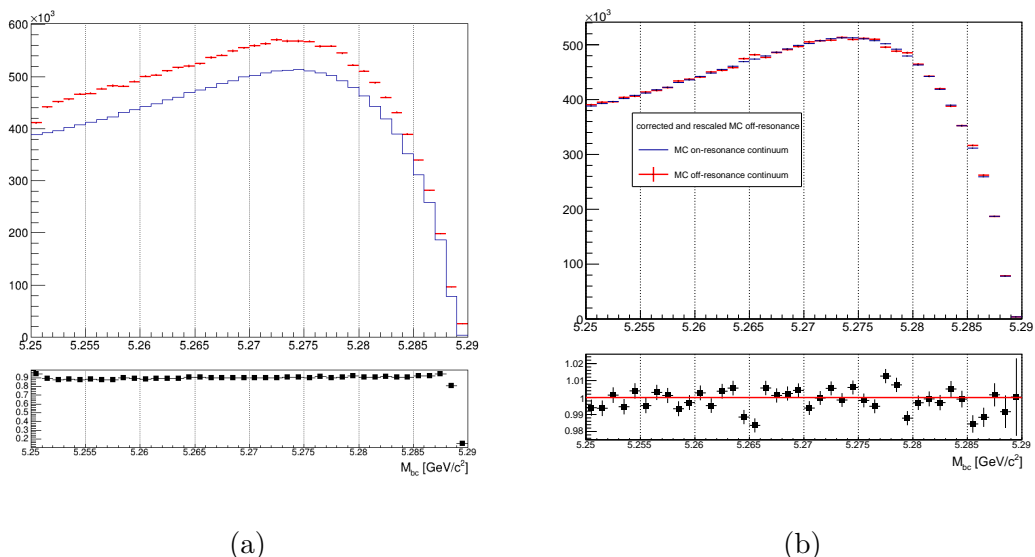


Figure (4.9) On the left: M_{bc} distributions of the MC off-resonance sample and the MC continuum sample with applied continuum suppression. On the right: M_{bc} distributions of the corrected scaled MC off-resonance and on-resonance MC continuum.

4.2 B_{tag} fit

An independent Monte Carlo stream was used to test the total fit model on tagged B meson candidates. As in the 2D fit, the parameter for the width, σ_{CB} , of the Crystal Ball is floated. The ratio between expected crossfeed background events and misreconstructed signal events is fixed from the MC. The misreconstructed signal PDF is also not fully constrained: the parameter describing the tail is free. To avoid introducing significant systematic uncertainties in the fit deriving from the M_{bc} endpoint region, where one has a smearing effect due to variations of the beam energy at the MeV level, the range for the fit is restricted to values between 5.250 and 5.287 GeV/c^2 .

4.2.1 Fit results for $B^- \rightarrow \Lambda_c^+$ decays

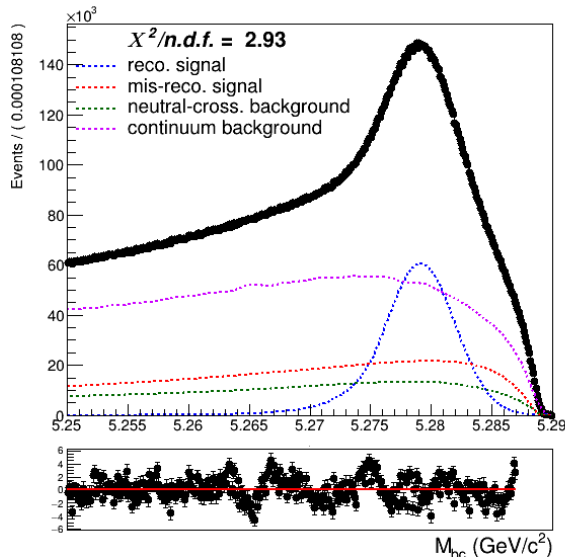


Figure (4.10) Total fit of tagged B mesons on Monte Carlo simulated data.

Yields for the reconstructed and misreconstructed signal are obtained from the fit:

	Fit results	expected
NrecSig	$4.7787 \cdot 10^6 \pm 6748$	$4.7571 \cdot 10^6 \pm 3214$
NmisSig	$5.3987 \cdot 10^6 \pm 5617$	$5.4035 \cdot 10^6 \pm 3376$

The normalization for the branching fraction is given by the NrecSig yields. The yields obtained in the fit differ by $\sim 3.2\sigma$ from the expected ones (obtained from a fit to the Total Signal events only). This discrepancy will impact the final measurement.

420 To check the stability of the fit model a toy MC study was performed with 3×10^3
 421 pseudo-datasets. No evidence for possible biases in the reconstructed signal yields was
 422 found (see Fig. 4.11).

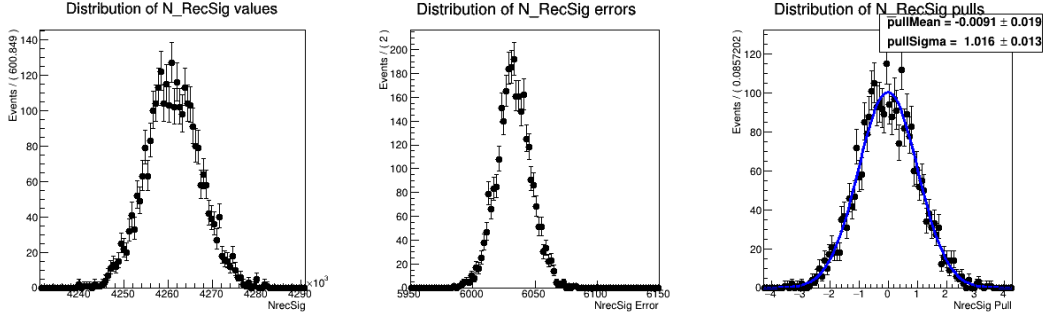


Figure (4.11) Plots showing distributions of the fitted signal yields, errors and the pull distribution of all pseudo-fits. (see Appendix ?? for the other free parameters' results)

423 4.2.2 Fit results for $B^- \rightarrow \bar{\Lambda}_c^-$ decays

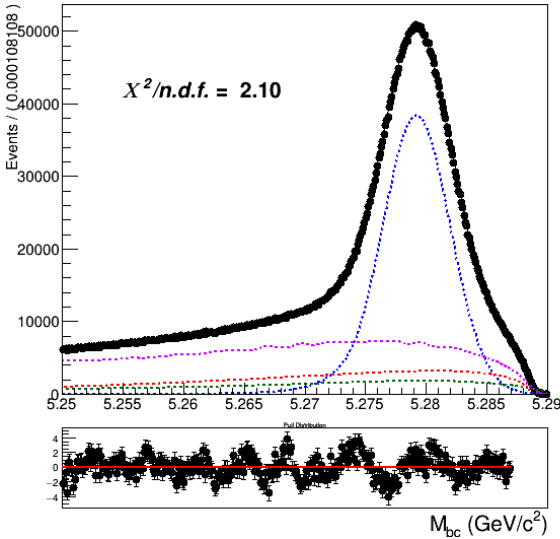


Figure (4.12) Total fit of tagged B mesons on Monte Carlo simulated data.

424

NrecSig	$2.5099 \cdot 10^6 \pm 4408$
NmisSig	$7.82307 \cdot 10^5 \pm 2936$

425 The Total Signal (the sum NrecSig+NmisSig) is 3292168 ± 2423 (to be compared with
 426 3299629 from the Monte Carlo), which means a $\sim 3\sigma$ underestimation. As in the case of

427 charged flavor-correlated decays, this can produce some systematic effect which needs to
 428 be taken into account.

429 But when performing a toy Monte Carlo study¹ the result show no bias on the
 430 reconstructed signal yields (see Fig. 4.13)

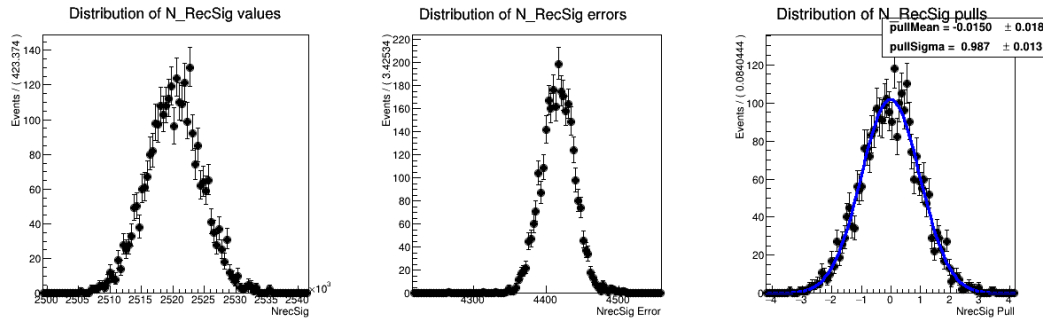


Figure (4.13) Plots showing distributions of the fitted signal yields, errors and the pull distribution of all pseudo-fits.

431 **4.2.3 Fit results for $\bar{B}^0 \rightarrow \Lambda_c^+$ decays**

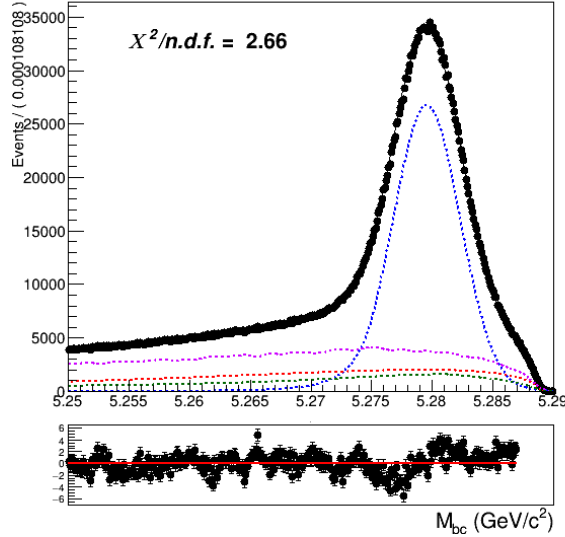


Figure (4.14) Total fit of tagged B mesons on Monte Carlo simulated data.

¹as usual performed with 3×10^3 pseudo-datasets

432 Reconstructed and misreconstructed signal yields obtained from the fit:

433

NrecSig	$1.7215 \cdot 10^6 \pm 3421$
NmisSig	$5.5950 \cdot 10^5 \pm 2215$

435 The Total Signal (the sum NrecSig+NmisSig) is 2281033 ± 1947 (to be compared with
 436 2286964 from the Monte Carlo). Also in this case it is an underestimated in the fit: $\sim 3\sigma$
 437 less.

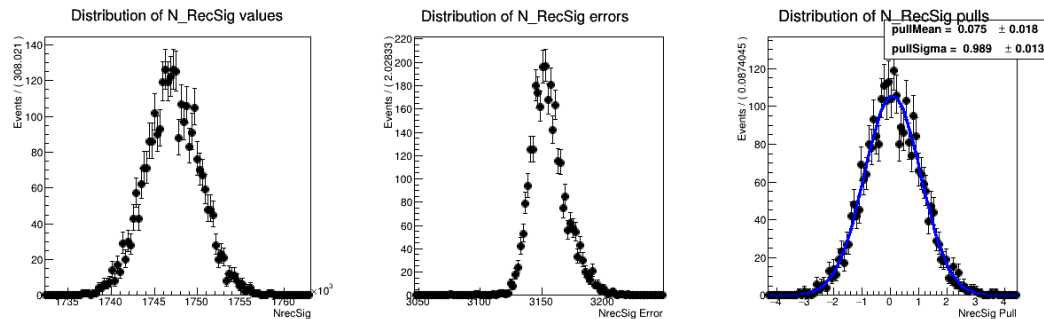


Figure (4.15) Plots showing distributions of the fitted signal yields, errors and the pull distribution of all pseudo-fits.

438 **4.2.4 Fit results for $B^0 \rightarrow \bar{\Lambda}_c^+$ decays**

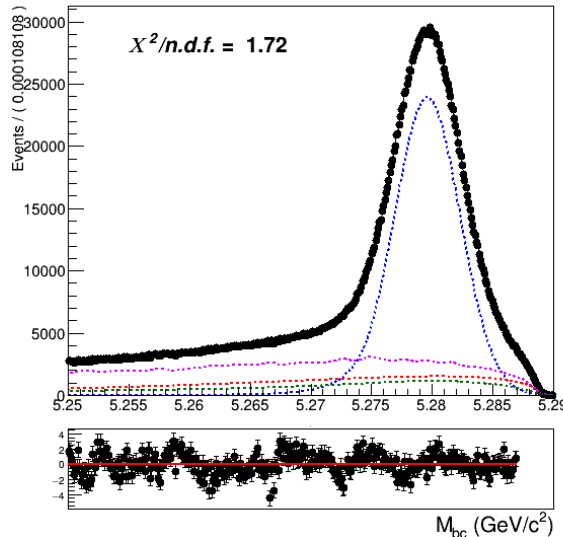


Figure (4.16) Total fit of tagged B mesons on Monte Carlo simulated data.

439 Reconstructed and misreconstructed signal yields obtained from the fit:

440

NrecSig	$1.5302 \cdot 10^6 \pm 3269$
NmisSig	$3.8332 \cdot 10^5 \pm 2072$

442 The Total Signal (the sum NrecSig+NmisSig) is 1913476 ± 1812 (to be compared with
443 1920156 from the Monte Carlo). Also in this case there is an underestimation of about a
444 $\sim 3.7\sigma$.

445 The toy MC study result for the signal yields is shown in Fig. 4.17. Also in this case
446 no hints of bias are visible.

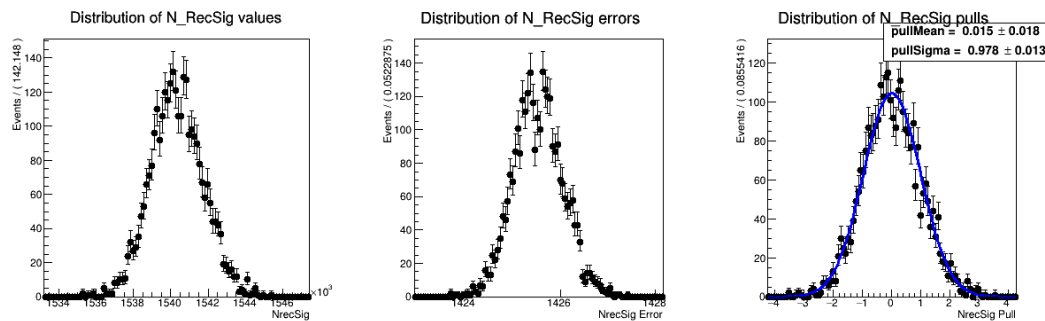


Figure (4.17) Plots showing distributions of the fitted signal yields, errors and the pull distribution of all pseudo-fits.

⁴⁴⁷ Chapter 5

⁴⁴⁸ Efficiencies

⁴⁴⁹ Here a decision was made not to rely on the estimated number of B meson pair, as it is
⁴⁵⁰ usually done, and the absolute FEI efficiency, since the latter shows large discrepancy
⁴⁵¹ between MC and data (see i.e. the results reported in the PhD Thesis by M. Gelb [?] and
⁴⁵² also by J. Schwab [?]) and also it depends strongly on the signal-side (i.e. $\epsilon_{FEI}^+ \neq \epsilon_{FEI,sig}^+$).
⁴⁵³ Instead, to limit the systematics, the branching ratio normalization is obtained using
⁴⁵⁴ the fitted tagged B mesons and the ratio $\epsilon_{FEI,sig}^+/\epsilon_{FEI}^+$ measured on MC, which one can
⁴⁵⁵ expect to be better described by the MC than the absolute FEI efficiency. The final
⁴⁵⁶ samples contain both signal and background candidates from various sources and in
⁴⁵⁷ order to extract N_{tag,Λ_c} and N_{tag} unbinned extended maximum-likelihood fits are performed.

⁴⁵⁸

⁴⁵⁹ 5.0.1 Λ_c efficiency

⁴⁶⁰ The efficiency of reconstructing the Λ_c baryon after correctly tagging the charged B
⁴⁶¹ meson, can be estimated from Monte Carlo simulated data. All available 10 streams of
⁴⁶² on-resonance Monte Carlo streams of simulated data were used to minimize statistical
⁴⁶³ uncertainties. The efficiency is evaluated as follows from the fraction:

$$\frac{N_{recSig}(B_{tag}, \Lambda_c)}{N_{recSig}(B_{tag}^{sig})} \quad (5.1)$$

⁴⁶⁴ where $N_{recSig}(B_{tag}, \Lambda_c)$ are the yields of reconstructed signal from a two dimensional fit of
⁴⁶⁵ corresponding inclusive decay. and $N_{recSig}(B_{tag}^{sig})$ are the yields of correctly reconstructed
⁴⁶⁶ signal from a fit of the tagged B mesons.

⁴⁶⁷ 5.0.2 $B^- \rightarrow \Lambda_c^+$ decays

$$\begin{aligned} \frac{\epsilon_{FEI,sig}^+}{\epsilon_{FEI}^+} &= 0.997 \pm 0.005 \\ \epsilon_{\Lambda_c} &= 37.78 \pm 0.45 \% \end{aligned}$$

470 **5.0.3** $B^- \rightarrow \bar{\Lambda}_c^-$ decays

471 $\frac{\epsilon_{FEI,sig}^+}{\epsilon_{FEI}^+} = 0.965 \pm 0.009$

472 $\epsilon_{\Lambda_c} = 42.39 \pm 0.66 \%$

473 **5.0.4** $\bar{B}^0 \rightarrow \Lambda_c^+$ decays

474 $\frac{\epsilon_{FEI,sig}^+}{\epsilon_{FEI}^+} = 1.090 \pm 0.010$

475 $\epsilon_{\Lambda_c} = 39.59 \pm 0.49 \%$

476 **5.0.5** $\bar{B}^0 \rightarrow \Lambda_c^-$ decays

477 $\frac{\epsilon_{FEI,sig}^+}{\epsilon_{FEI}^+} = 1.005 \pm 0.014$

478 $\epsilon_{\Lambda_c} = 41.49 \pm 1.13 \%$

479

Chapter 6

480

Branching ratio

	total fit	signal fit	BELLE MC VALUE
stream 0	(2.84 ± 0.13)%	(2.96 ± 0.07)%	(2.91 ± 0.03)%
stream 1	(2.82 ± 0.14)%	(2.99 ± 0.07)%	(2.91 ± 0.03)%
stream 2	(2.97 ± 0.14)%	(2.97 ± 0.07)%	(2.90 ± 0.03)%
stream 3	(2.76 ± 0.14)%	(2.90 ± 0.07)%	(2.91 ± 0.03)%
stream 4	(3.06 ± 0.14)%	(3.05 ± 0.07)%	(2.90 ± 0.03)%
stream 5	(2.83 ± 0.14)%	(2.84 ± 0.07)%	(2.92 ± 0.03)%
average	(2.88 ± 0.06)%	(2.95 ± 0.03)%	(2.91 ± 0.01)%

Table (6.1) charged corr

	total fit	signal fit	BELLE MC VALUE
stream 0	(1.24 ± 0.11)%	(1.19 ± 0.05)%	(1.217 ± 0.002)%
stream 1	(1.24 ± 0.11)%	(1.21 ± 0.05)%	(1.218 ± 0.002)%
stream 2	(1.35 ± 0.12)%	(1.23 ± 0.05)%	(1.218 ± 0.002)%
stream 3	(1.16 ± 0.10)%	(0.20 ± 0.05)%	(1.215 ± 0.002)%
stream 4	(1.44 ± 0.13)%	(1.21 ± 0.05)%	(1.218 ± 0.002)%
stream 5	(1.04 ± 0.11)%	(1.15 ± 0.05)%	(1.217 ± 0.002)%
average	(1.25 ± 0.05)%	(1.20 ± 0.02)%	(1.217 ± 0.001)%

Table (6.2) charged anticorr

481

Bibliography

- 482 [1] B. Aubert et al., BaBar, *Study of inclusive B^- and \bar{B}^0 decays to flavor-tagged D , D_s and Λ_c^+* , Phys. Rev. D **75** (2007) 072002, [arXiv:hep-ex/0606026](https://arxiv.org/abs/hep-ex/0606026).
- 483
- 484 [2] I. Grach, I. Narodetskii, S. Simula, and K. Ter-Martirosyan, *Exclusive and inclusive weak decays of the B -meson*, Nuclear Physics B **502** (1997) no. 1-2, 227–248.
- 485
- 486 [3] Y. Hsiao, S.-Y. Tsai, C.-C. Lih, and E. Rodrigues, *Testing the W -exchange mechanism with two-body baryonic B decays*, Journal of High Energy Physics **2020** (apr, 2020) .
487 [https://doi.org/10.1007/JHEP04\(2020\)035](https://doi.org/10.1007/JHEP04(2020)035).
488